Meteoritics & Planetary Science 37, 1107–1128 (2002)
Available online at http://www.uark.edu/meteor

Martian meteorite Dhofar 019: A new shergottite

L. A. TAYLOR[1]*, M. A. NAZAROV[1,2], C. K. SHEARER[3], H. Y. MCSWEEN, JR.[1], J. CAHILL[1], C. R. NEAL[4], M. A. IVANOVA[2], L. D. BARSUKOVA[2], R. C. LENTZ[1], R. N. CLAYTON[5] AND T. K. MAYEDA[5]

[1]Planetary Geosciences Institute, Department of Geological Sciences, University of Tennessee, Knoxville, Tennessee 37996-1410, USA
[2]Vernadsky Institute of Geochemistry and Analytical Chemistry, Russian Academy of Sciences, Kosygin St. 19, Moscow 117975, Russia
[3]Institute of Meteoritics, University of New Mexico, Albuquerque, New Mexico 87131, USA
[4]Department of Civil Engineering and Geological Sciences, University of Notre Dame, Notre Dame, Indiana 46556, USA
[5]Enrico Fermi Institute, University of Chicago, Chicago, Illinois 60637, USA
*Correspondence author's e-mail address: lataylor@utk.edu

(Received 2001 August 29; accepted in revised form 2002 May 13)

Abstract–Dhofar 019 is a new martian meteorite found in the desert of Oman. In texture, mineralogy, and major and trace element chemistry, this meteorite is classified as a basaltic shergottite. Olivine megacrysts are set within a groundmass composed of finer grained olivine, pyroxene (pigeonite and augite), and maskelynite. Minor phases are chromite-ulvöspinel, ilmenite, silica, K-rich feldspar, merrillite, chlorapatite, and pyrrhotite. Secondary phases of terrestrial origin include calcite, gypsum, celestite, Fe hydroxides, and smectite.

Dhofar 019 is most similar to the Elephant Moraine (EETA) 79001 lithology A and Dar al Gani (DaG) 476/489 shergottites. The main features that distinguish Dhofar 019 from other shergottites are lack of orthopyroxene; lower Ni contents of olivine; the heaviest oxygen-isotopic bulk composition; and larger compositional ranges for olivine, maskelynite, and spinel, as well as a wide range for pyroxenes. The large compositional ranges of the minerals are indicative of relatively rapid crystallization. Modeling of olivine chemical zonations yield minimum cooling rates of 0.5–0.8 °C/h. Spinel chemistry suggests that crystallization took place under one of the most reduced conditions for martian meteorites, at an fO_2 3 log units below the quartz-fayalite-magnetite (QFM) buffer.

The olivine megacrysts are heterogeneously distributed in the rock. Crystal size distribution analysis suggests that they constitute a population formed under steady-state conditions of nucleation and growth, although a few grains may be cumulates. The parent melt is thought to have been derived from partial melting of a light rare earth element- and platinum group element-depleted mantle source. Shergottites, EETA79001 lithology A, DaG 476/489, and Dhofar 019, although of different ages, comprise a particular type of martian rocks. Such rocks could have formed from chemically similar source(s) and parent melt(s), with their bulk compositions affected by olivine accumulation.

INTRODUCTION

Shergottites, nakhlites, and Chassigny (SNC), and Allan Hills (ALH) 84001 meteorites are igneous rocks believed to have come from Mars. Martian meteorites have been studied extensively to provide possible petrologic constraints on the geological history of Mars (*e.g.*, McSween, 1994, 2002). Among these meteorites, basaltic shergottites (Shergotty, Zagami, Queen Alexandra Range (QUE) 94201, Elephant Moraine (EETA) 79001A (= lithology A), Dar al Gani (DaG) 476/489, Los Angeles) are distinct from lherzolitic shergottites (ALHA77005, Lewis Cliff (LEW) 88516, Yamato (Y)-793605) in that the latter contain much larger amounts of olivine and are considered to be cumulate rocks.

Dhofar 019 is a new shergottite member of the martian meteorite group. This 1.06 kg meteorite was recovered from the Dhofar region of Oman on 2000 January 24. In this paper, we report mineralogy, petrology, major and trace element chemistry, and oxygen-isotopic compositions of this shergottite. Taylor *et al.* (2000) and Shearer *et al.* (2000) have presented preliminary results, in addition to abstracts by Badjukov *et al.* (2001), Folk and Taylor (2000), Folk *et al.* (2001), Neal *et al.* (2001), Shearer *et al.* (2001), Mikouchi and Miyamoto (2001), and Cahill *et al.* (2002).

METHODOLOGY

Polished thick and thin sections (50 mm^2 area) of Dhofar 019 were studied by both reflected- and transmitted-light microscopy. Electron microprobe analyses were performed at the University of Tennessee with a Cameca SX50, operated at

Prelude preprint MS#4638

15 kV and 20 nA, with a 1–5 μm spot size, and 20 s count times. Mineral modes were measured using an Oxford Instrument energy-dispersive analysis (EDS) unit, using FeatureScan software, as outlined by Taylor *et al.* (1996). At the Vernadsky Institute, a representative 1 g sample was crushed and powdered in an agate mortar for bulk-rock major and trace element determinations: x-ray fluorescence (XRF) and inductively-coupled plasma (ICP) analyses for major elements, wet chemistry for Fe^{2+} and Fe^{3+} contents, atomic absorption for Na and K, combustion analyses for C and S, and instrumental neutron activation analysis (INAA) for trace elements (rare earth elements (REEs), Sc, Co, Cr). Another 115 mg portion was studied, from which samples of 9.5 and 105.5 mg were used. The larger portion was powdered in an agate mortar under clean-room conditions at the University of Notre Dame. The 9.5 mg sample was dissolved using HF/HNO_3 for major and trace element analysis by inductively-coupled plasma-mass spectrometry (ICP-MS). The resulting solution was analyzed twice for trace elements at different dilutions to check for reproducibility, because many incompatible trace elements were present at the submicrogram per gram level. For both major and trace element determinations, reference material BHVO-1 was also analyzed. The remaining powder (105.5 mg) was dissolved for platinum group element (PGE) analysis following the method of Ely *et al.* (1999). Reference material UMT-1 was run with Dhofar 019 to check column yield and accuracy. Another separate split of Dhofar 019, weighing ~10 mg, was used to measure bulk oxygen-isotopic compositions at the University of Chicago, following the procedure of Clayton and Mayeda (1983).

Trace elements in olivine, pyroxene, maskelynite, and phosphates were measured using the Cameca ims 4f secondary ion mass spectrometer (SIMS), operated by the University of New Mexico-Sandia National Laboratories consortium. Analyses were made using primary O^- ions accelerated through a nominal potential of 10 kV. A primary beam current of 15 to 35 nA was focused on the sample over a spot diameter of 10 to 40 μm. Sputtered secondary ions were energy filtered using a sample-offset voltage of 105 V for Sc, Ti, V, Cr, Co, and Ni, and a sample offset voltage of 75 V for REE. For both sets of analytical conditions, an energy window of 50 V was used. Analyses involved repeated cycles of peak counting. The analytical procedure included counting on a background position to monitor detection noise. Absolute concentrations of each element in silicates were calculated using empirical relationships of trace element/$^{30}Si^+$ ratios (normalized to known SiO_2 content) as compared to element concentrations, as derived from daily calibration. Absolute concentrations of trace elements in phosphate were calculated using empirical relationships of each element to Ca. Calibration curves were constructed using well-documented olivine, pyroxene, plagioclase, and apatite standards.

PETROGRAPHY

Dhofar 019 is a brownish-gray, angular meteorite fragment that is roughly 12 × 9 × 8 cm in size and weighs 1056 g (Fig. 1). Fusion crust is virtually absent, apparently destroyed by wind abrasion. The bottom portion of the meteorite, which was

FIG. 1. The Dhofar 019 stone. The bottom (light) portion of the stone was burried in the caliche soil. The cube is 1 cm on an edge.

buried in caliche soil, has a yellowish-white color. This portion is covered with sand and caliche, cemented by carbonate material. However, freshly cut interior surfaces are greenish-gray.

Cut slices of Dhofar 019 show a heterogeneous, largely equigranular rock with a basaltic texture (Fig. 2). Some thin sections contain additional large (1–3 mm) olivine megacrysts. The average grain size of most of the rock is 0.2–0.5 mm. Although having a grain size similar to that in Shergotty and Zagami (*e.g.*, Meyer, 1998), Dhofar 019 has no foliation, as developed in Shergotty and Zagami (Stolper and McSween, 1979; McCoy *et al.*, 1992).

Pale-brown pyroxene, mostly granular or lath shaped (Fig. 2), is the most abundant mineral (~64 vol%). The pyroxene is mainly pigeonite; augite is less abundant and occurs mainly as overgrowths on pigeonite cores, or as individual subhedral grains. Some augite crystals are also mantled by later pigeonite. Plagioclase has been completely converted to maskelynite (feldspathic glass) and is mostly interstitial (Fig. 3a). Olivine is distinctively yellow to brown and typically forms large subhedral megacrysts or clusters of a few individual grains (≤1–3 mm; Fig. 3a,b). However, olivine is also present as small anhedral grains in the matrix of the meteorite. Most olivine megacrysts contain melt inclusions (≤0.2 mm in size) consisting mainly of a glass and augite (Fig. 3b). Augite partially envelops the inclusions, as well as forming skeletal crystals in the glass. These melt inclusions are similar to those described in DaG 489 (Folco *et al.*, 2000).

As demonstrated below, both the major and trace element chemistry of the megacrysts and the groundmass olivines are similar, leading to the conclusion that the megacrysts are phenocrysts. However, below, we present evidence that some of the olivine grains may be of cumulate origin. Therefore, we will use the term megacrysts, which does not have a genetic connotation.

Accessory minerals are chromite-ulvöspinel, ilmenite, silica, K-rich feldspar, merrillite (whitlockite), chlorapatite, and pyrrhotite. Chromite is present as euhedral grains (≤0.15 mm), commonly mantled by Cr-rich ulvöspinel, displaying a fine-exsolution texture (Fig. 3c). Separate grains of Cr-rich ulvöspinel are also present, associated with late-stage phases. Ilmenite occurs as anhedral or lath-shaped grains (Fig. 3d,e). Phosphates show anhedral to lath-like shapes and tend to be associated with areas of late-stage mesostasis. Small blebs of K-feldspar and a silica phase also occur in this mesostasis. Anhedral pyrrhotite grains are usually less than 20–30 μm in size, often located at feldspar/pyroxene borders (Fig. 3a,d,e), but pyrrhotite inclusions also occur in all major phases. The sequence of crystallization inferred from textural relationships in Dhofar 019 is olivine + chromite ⇒ pigeonite + Ti-chromite ⇒ pigeonite + augite + plagioclase + Cr-rich ulvöspinel + ilmenite ⇒ mesostasis.

Weathering products include calcite, gypsum, celestite, Fe hydroxides, and smectite. Calcite is most abundant and present mainly as veins cross-cutting the meteorite. Some Fe hydroxides are associated with pyrrhotite weathering, but most is present in minute veins around and through olivine grains, resulting in

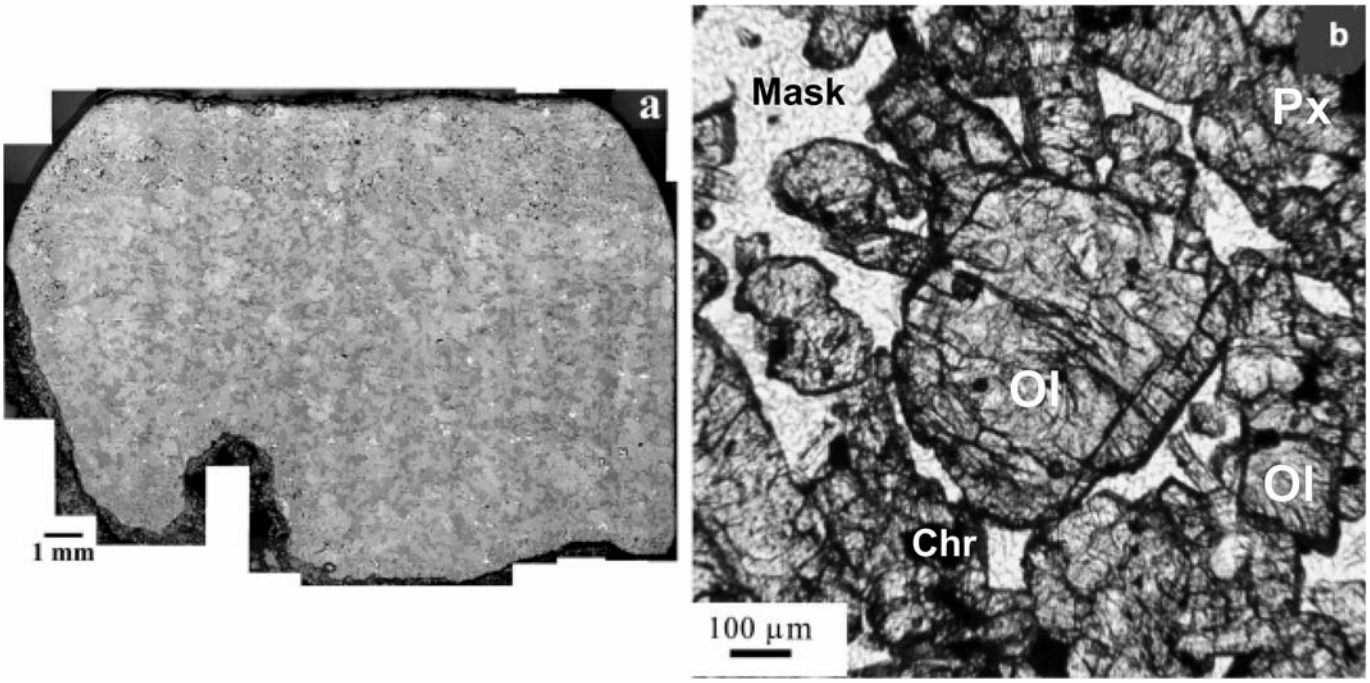

FIG. 2. Optical microscope images of a thin section of Dhofar 019 in (a) reflected and (b) transmitted light. The rock is somewhat heterogeneous and largely equigranular. In reflected light (a), the layer in the upper part of the photo appears finer grained, a result of having the abundant terrestrial calcite dissolved out. In (b), an olivine (Ol) megacryst is set within a matrix of smaller olivine, pyroxene (Px), maskelynite (Mask), and chromite-ulvöspinel (Chr) grains.

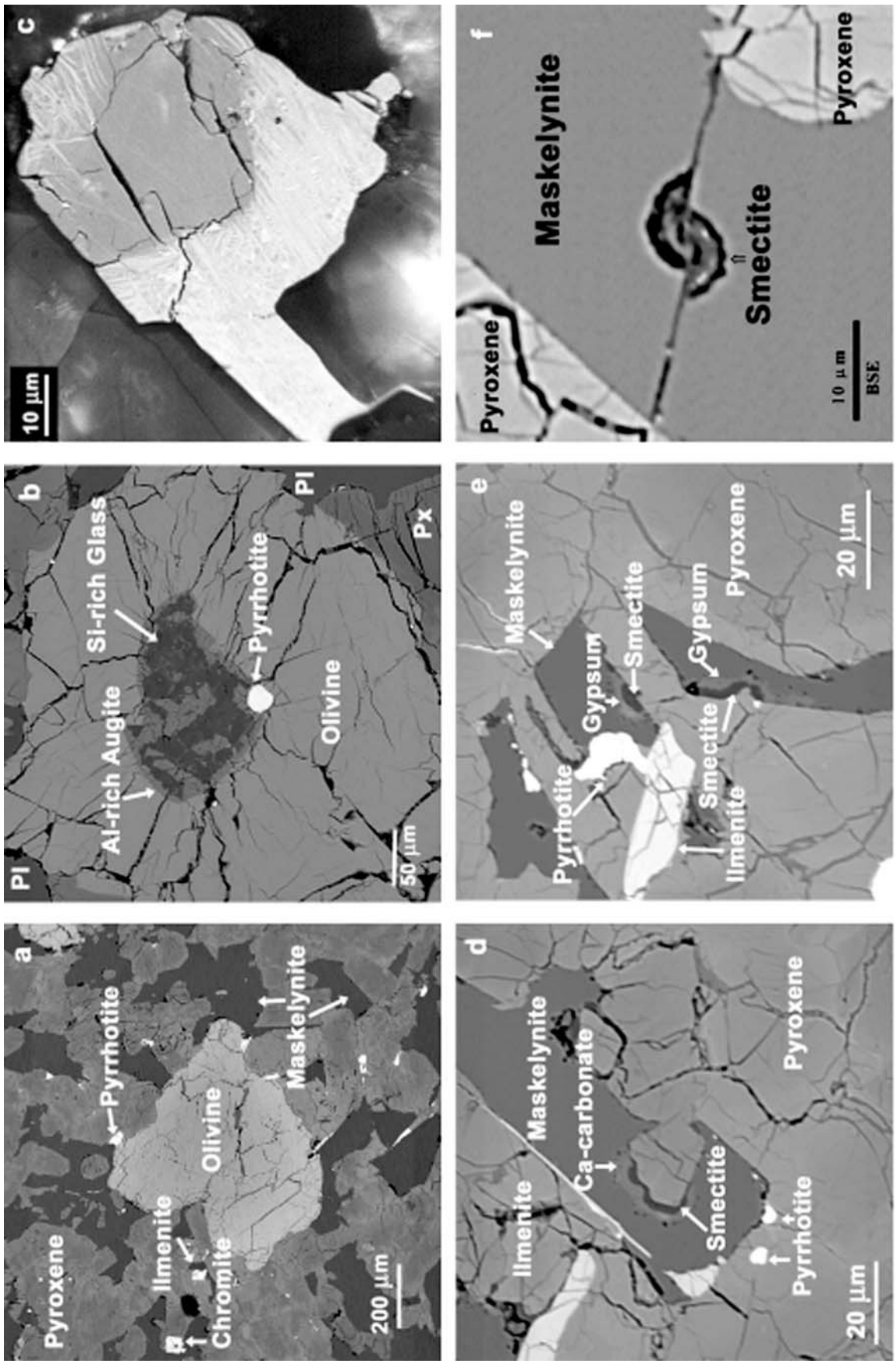

FIG. 3. Photomicrographs from a Dhofar 019 thin section. (a) Backscattered electron (BSE) image of an olivine megacryst; (b) a BSE image of a melt inclusion set in an olivine megacryst; (c) chromite (dark) is commonly mantled by Cr-rich ulvöspinel, displaying a fine-exsolution texture (reflected light, oil immersion); (d) BSE image of secondary terrestrial minerals of smectite and calcite; (e) same as (d) but with gypsum instead; and (f) smectite, cut and intersected by right-lateral, micro-faulting of maskelynite, which suggests at least some of the smectite may have formed on Mars.

a distinctive stain to the olivine grains. Other secondary phases are located mainly at maskelynite borders with pyroxenes. They commonly form mineralogically zoned grains, which appear to replace maskelynite (Fig. 3d,e). Such secondary minerals at boundaries with pyroxene consist mainly of smectite, with their outer portions composed of gypsum and/or calcite. The microfaulting, apparently through the smectite in the plagioclase in Fig. 3f, possibly occurred during the launch from Mars or upon impact on Earth. This suggests that at least some of the smectite in this rock may be of extraterrestrial origin.

Quantitative Petrography

Two different techniques, crystal size distribution (CSD) and cluster analysis, were applied to quantify the olivine textural data and to help constrain the petrogenesis of this phase. CSD theory holds that the shape of a plot of the log of the grain number density *vs.* grain size for a given population of grains will indicate the geologic processes involved in the formation of that population (Marsh, 1988). For example, the simplest CSD plot of a negative linear slope indicates the population grew under steady-state conditions of nucleation and growth, where the slope is inversely related to the product of the growth rate and the residence time of the grains ($m = 1/G\tau$) (Marsh, 1988). Deviations from linearity suggest the involvement of such geologic processes as crystal accumulation (concave-up) or solid-state annealing (concave-down) during formation of the grain population.

For the CSD analysis, widths of 898 olivine grains from three thin sections were measured on combined Fe and Mg distribution maps. Of all these grains, only six were >0.6 mm, and only one of those was >1 mm (a single megacryst). On the CSD plot (Fig. 4a), the rest of the grain population describes a well-defined linear curve, with only a minor turnover at the smallest grain size. The slope of a best-fit line ($R^2 = 0.994$) to this plot is –21.7/mm. The linearity of the plot most likely implies steady-state conditions of nucleation and growth, perhaps with some subsequent minor annealing to produce the small turnover. The few larger grains may represent olivine cumulates from the early portion of melt crystallization.

The cluster analysis method we used was derived by Jerram *et al.* (1996). It is a practical method for applying standard statistical cluster analysis to geologic samples to distinguish between ordered and clustered distributions, when compared to a random distribution. The critical measurement for applying this technique is locating all the grain centers in a sample and finding the average nearest neighbor distance between centers (r_A). This average distance is then compared to the equivalent average for a randomly distributed population of the same area and grain density, or porosity, (r_E). This yields the key parameter R from $R = r_A/r_E$. Values of R derived from several populations of randomly distributed spheres produce a reference line that separates ordered and clustered distributions (Jerram *et al.* 1996), the random sphere distribution (RSD) line shown in Fig.4b. For this study, only one thin section (with 342 olivine grains) was analyzed, but the results clearly show that the population of small olivines in Dhofar 019 falls well within the "clustered" portion of the graph (Fig. 4b). According to Jerram *et al.* (1996), this implies that the olivine grains either grew from clusters of nuclei or accumulated in clusters, rather than as individual, randomly distributed grains.

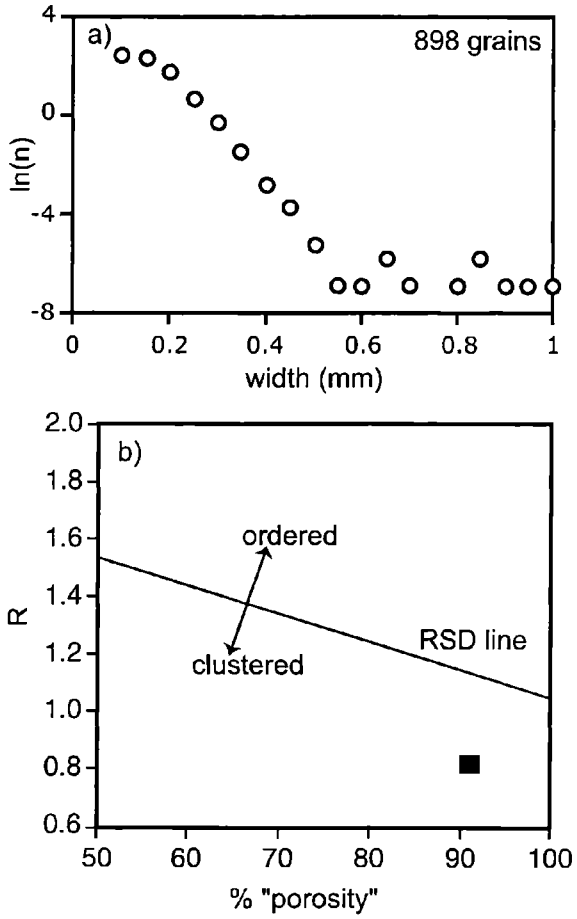

FIG. 4. Quantitative petrographic analyses. (a) Crystal size distribution plot of grain size *vs.* log of the grain number density for olivine grains from three Dhofar 019 thin sections. Note the linearity over sizes up to 0.6 mm, indicating a single population grown under steady-state conditions of nucleation and growth. The ragged tail towards larger grain sizes represents only six grains, possibly of a distinct population. (b) Cluster analysis results from one thin section indicating the clustered nature of the Dhofar olivines. Definition of R in text. Note that "porosity", as used here, is that portion of the rock that is *not* olivine (*i.e.*, total – modal% olivine).

Based upon its texture and modal mineralogy (Table 1), Dhofar 019 is a shergottite member of the martian rock group. Although its high-olivine content is atypical, Dhofar 019 is hereby classified as a *basaltic shergottite*. However, in contrast to the shergottites EETA79001A and DaG 476/489, Dhofar 019 is richer in feldspathic glass and does not contain orthopyroxene megacrysts. In addition, EETA79001A and DaG 476/489 are very similar in CSD (Lentz and McSween, 2000), although

TABLE 1. Modal abundances of minerals in Dhofar 019 and other shergottites (vol%).

	Dhofar 019		Shergottites		
	Average	Range of three thin sections	Basaltic shergottites*	"Olivine-bearing" shergottites†	Lherzolitic shergottites‡
Olivine	10.1	6.6–12.3	0.3–4.0	7–17	35–60
Orthopyroxene	n.d.§	n.d.	n.d.	1.5–7.0	tr.–25
Clinopyroxene	61.4	57.2–62.6	38–80	55–65	4–60
Plagioclase	26.1	25.7–27.4	10–48	14–18	5–9
Opaque phases	1.8	1.6–2.0	2–5	3	1–2
Chromite	0.6	0.4–0.7	–	–	–
Ulvöspinel	0.4	0.3–0.4	–	–	–
Ilmenite	0.4	0.3–0.5	–	–	–
Pyrrhotite	0.4	0.3–0.4	–	–	–

*The ranges are for Shergotty, Zagami, Los Angeles, Queen Alexandra Range 94201, and Elephant Moraine (EET) A79001B (Meyer, 1998; Rubin *et al.*, 2000).
†The ranges are for Dar al Gani 476/489 and EETA79001A (Meyer, 1998; Zipfel *et al.*, 2000; Folco *et al.*, 2000).
‡The ranges are for Lewis Cliff 88516, Allan Hills A77005, Yamato-793605 (Meyer, 1998).
§Not detected (<0.2%).
Abbreviation: tr. = trace.

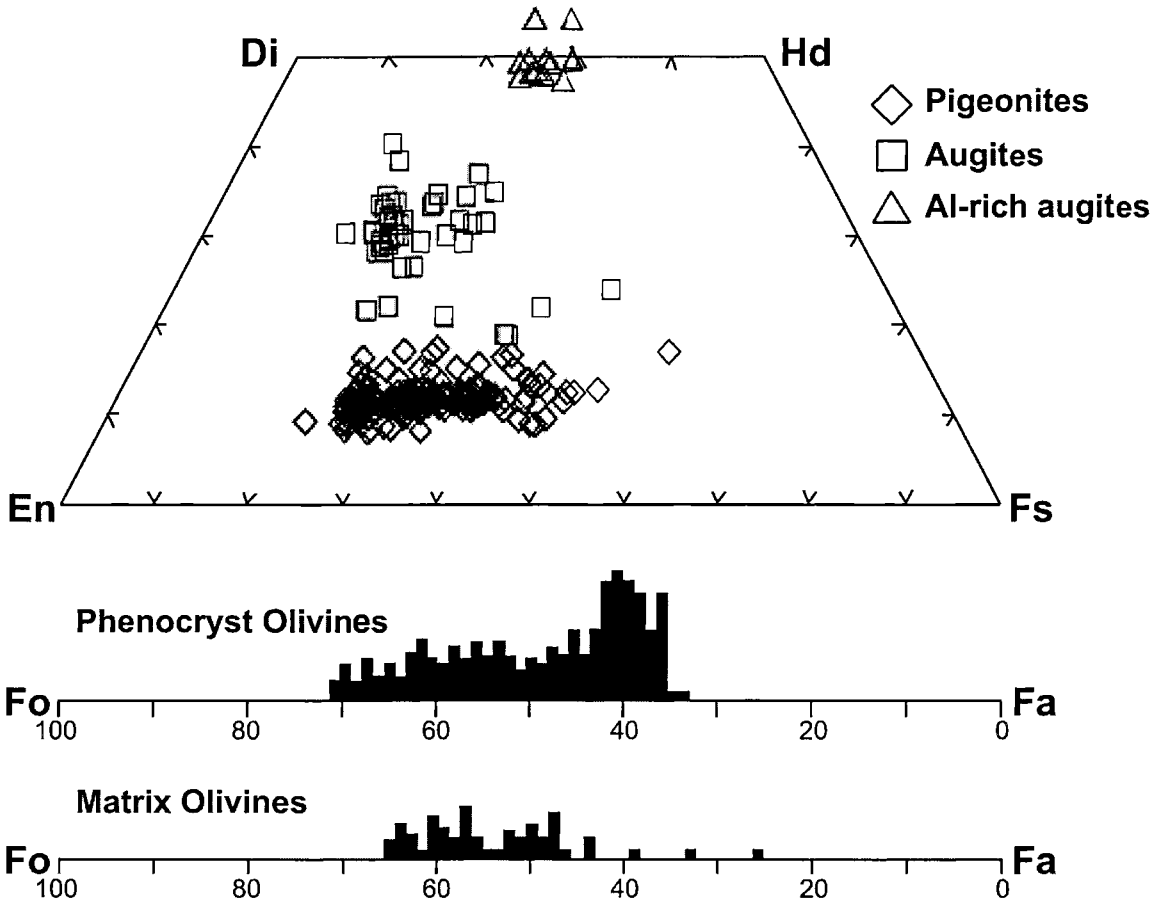

FIG. 5. Pyroxene and olivine compositions in Dhofar 019. Olivine has a large range from Fo_{72} to Fo_{25}. Note also that olivine phenocrysts overlap those of those of the finer grained, matrix olivines.

EETA79001A has been suggested to be the result of impact melting (*e.g.*, Mittlefehldt *et al.*, 1999).

MINERAL CHEMISTRY

Pyroxene

Pyroxenes are normally zoned, with pigeonite compositions in the range of $Wo_{9-15}En_{40-70}$, and augite in the range $Wo_{30-40}En_{40-50}$ (Fig. 5). Contents of Al_2O_3, Cr_2O_3, and TiO_2 (Table 2) are typical for SNC pyroxenes. Contents of Cr_2O_3 decrease with an increase in *Fe#* [Fe/(Fe + Mg)], whereas TiO_2 increases slightly (Fig. 6). No orthopyroxene was detected. The Fe/Mn ratios of pyroxenes are similar to those of SNCs. In general, the Dhofar 019 pyroxenes overlap in composition both those in lherzolitic shergottites and basaltic shergottites and are similar to pyroxenes in Shergotty.

There are two distinct sets of augites. Besides the major augite associated with the pigeonite, Al-rich augites occur in melt inclusions within megacrystic olivines and contain up to 16 wt% Al_2O_3 and 3 wt% TiO_2 (Table 2; Fig. 6), with salite-like compositions (Fig. 5). These augites are stoichiometric. The Al-rich augites have similar compositions to those also reported from melt inclusions in other SNC meteorites (Floran *et al.*, 1978; Jagoutz, 1989; Harvey *et al.*, 1993; Folco *et al.*, 2000).

The pyroxenes have lower Ni (100–200 ppm) (Fig. 7) and substantially higher V, Cr (Fig. 8), and REE (Fig. 9) than the olivine. The pigeonite has a light (L)REE-depleted pattern with a possible minor negative-Eu anomaly. Although Ce anomalies have been reported in pigeonite from other desert martian meteorites (Crozaz and Wadhwa, 2001; Wadhwa *et al.*, 2001), there are no Ce anomalies, outside analytical error, in pyroxene from Dhofar 019. Overall, REE concentrations of pigeonite

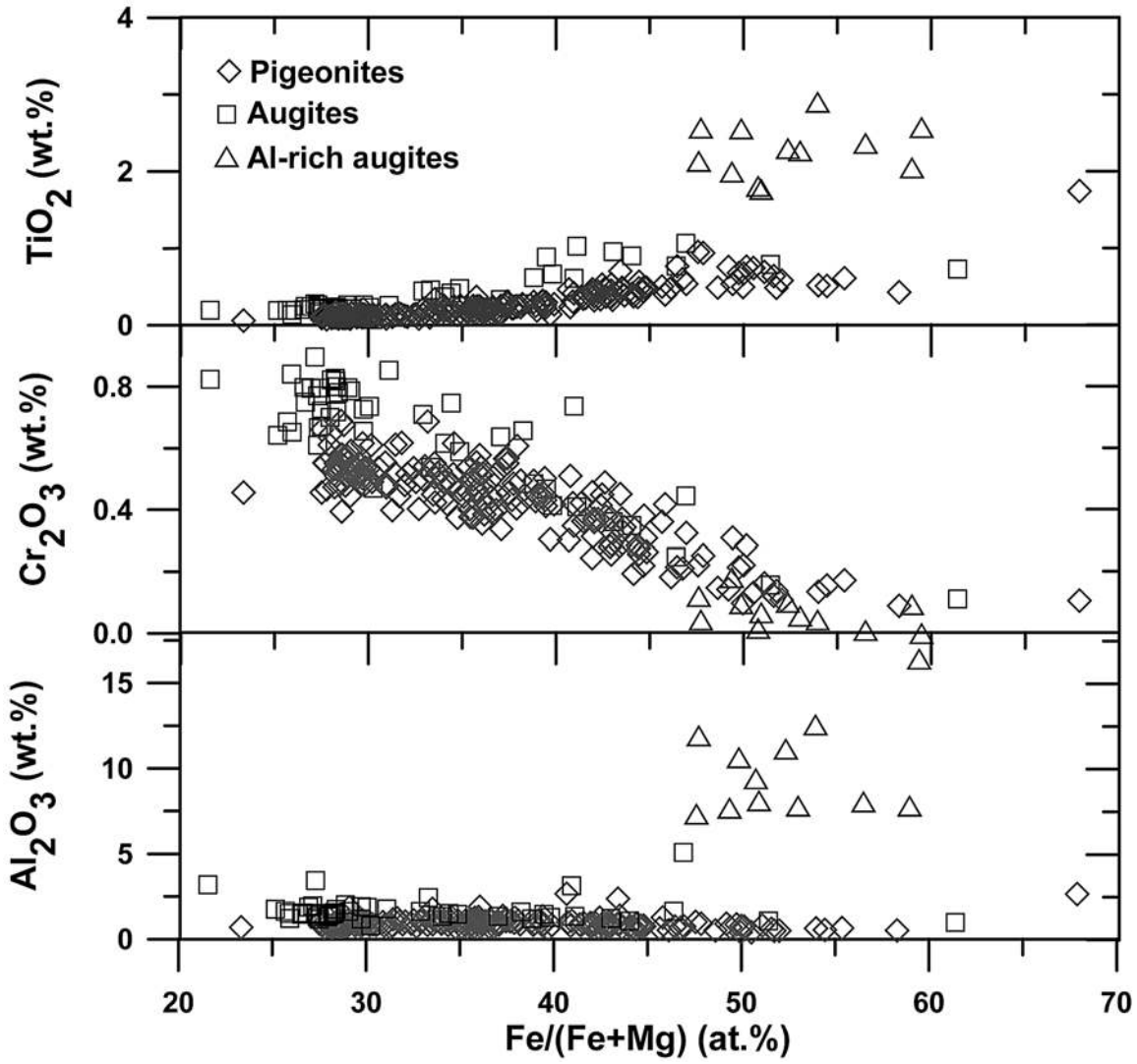

FIG. 6. Concentrations of Al_2O_3, Cr_2O_3, and TiO_2 in pyroxenes of Dhofar 019. The Ti content increases slightly with increasing Fe/(Fe + Mg), whereas Cr content decreases with increasing Fe/(Fe + Mg). Note the Al-rich augite of melt inclusions, enriched in Al and Ti.

TABLE 2. Representative electron microprobe analyses of major minerals in Dhofar 019.

	Pigeonite		Augite	Al-rich augite	Olivine		Maskelynite		
	Core	Rim			Core	Rim	Ca-rich	Na-rich	K-rich
SiO_2	53.3	51.1	52.6	40.0	36.1	34.1	51.2	60.0	70.4
TiO_2	0.12	0.50	0.21	2.57	0.02	0.03	<0.03	<0.03	<0.03
Al_2O_3	0.80	0.63	1.40	16.4	0.02	<0.03	29.8	25.3	15.9
Cr_2O_3	0.49	0.36	0.72	<0.03	0.06	0.03	<0.03	<0.03	<0.03
FeO*	17.4	24.1	11.6	13.2	34.9	44.9	1.05	0.49	0.87
MnO	0.55	0.70	0.44	0.31	0.62	0.74	<0.03	<0.03	<0.03
MgO	22.5	16.1	17.1	5.06	28.3	20.0	<0.03	<0.03	<0.03
CaO	4.40	5.62	15.5	20.6	0.32	0.27	13.4	7.07	1.06
Na_2O	0.05	0.05	0.13	0.24	0.01	0.03	3.52	6.25	3.00
K_2O	<0.03	–	<0.03	<0.03	<0.03	<0.03	0.15	0.98	7.20
Total	99.6	99.2	99.7	98.4	100.3	100.1	99.1	100.1	98.4
Fo	–	–	–	–	59.1	44.2	–	–	–
Wo/An	8.9	12.0	32.0	54.3	–	–	67.0	36.1	7.0
Fs/Ab	27.5	40.2	18.7	27.2	–	–	32.0	57.9	36.1

	Silica	Ilmenite	Chromite			Merrillite (whitlockite)	Apatite	Mg-rich smectite	Fe-rich smectite
			Core	Rim					
SiO_2	97.3	0.03	0.15	0.02	0.03	0.09	0.55	41.7	42.7
TiO_2	<0.03	52.6	0.92	22.5	28.6	–	–	0.07	0.34
Al_2O_3	1.03	0.04	9.64	3.99	2.98	0.01	0.15	14.5	0.64
Cr_2O_3	–	0.41	54.1	19.9	6.57	–	–	0.06	0.18
FeO*	0.36	43.8	30.9	50.7	58.9	1.84	0.96	0.95	13.9
MnO	–	0.64	0.38	0.59	0.66	0.07	0.21	0.08	0.44
MgO	<0.03	1.75	3.16	2.03	1.34	3.10	0.30	24.5	14.7
CaO	0.10	–	–	–	–	47.9	56.4	1.72	3.37
Na_2O	0.28	–	–	–	–	1.00	0.26	<0.03	0.06
K_2O	–	–	–	–	–	0.03	0.03	<0.03	<0.03
P_2O_5	–	–	–	–	–	45.6	39.6	–	–
Cl	–	–	–	–	–	<0.03	2.39	–	–
Total	99.1	99.3	99.2	99.8	99.1	99.6	100.8	83.6	76.3
FeO†	–	–	28.6	48.3	54.2	–	–	–	–
Fe_2O_3†	–	–	2.16	1.50	3.93	–	–	–	–

*Total Fe as FeO.
†Calculated from stoichiometry.

overlap the higher portion of the range previously observed in lherzolitic and basaltic shergottites (Borg *et al.*, 2001; Wadhwa, 2001). Compared to pigeonite, augite has higher REE, Sc and Ti, a flatter REE pattern, and lower Co and Ni. The REE patterns flatten, and abundances increase, as the Al content of augite increases. There is no discernible relationship between the enstatite component in the augite and REE characteristics, in agreement with previous studies (McKay, 1986).

Olivine

Olivines have compositions of Fo_{73-25}. Some megacryst olivine crystals are zoned from cores of Fo_{70} to rims of Fo_{50} (Table 2). Small grains are individually homogeneous, yet define a similar overall compositional range (Fig. 5). Compared to other martian meteorites, olivines of Dhofar 019 have an exceptionally wide range of compositions (Fig. 10). These olivines extend to more Fe-rich compositions compared to olivines from lherzolitic shergottites, basaltic shergottites (DaG 476/489 and EETA79001A), Chassigny, and ALHA84001. Conversely, they are richer in Mg compared to olivines from nakhlites and the other basaltic shergottites. As expected, the Fe/Mn ratios of the olivines are also higher than those of pyroxenes. Contents of CaO vary from 0.16 to 0.55 wt%, with an average of 0.35 wt%. These concentrations are characteristic of olivines in extrusive rocks (Smith *et al.*, 1983).

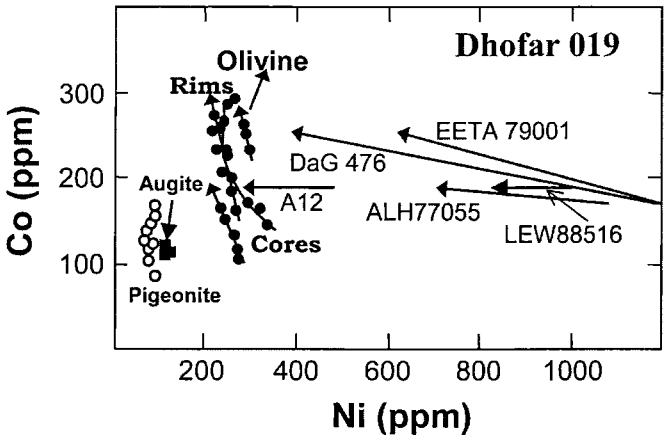

FIG. 7. The contents of Co *vs.* Ni for pyroxene and olivine in Dhofar 019. Also included are trajectories for olivine crystallization trends from core to rims from other martian meteorites and Apollo 12 basalts (Herd *et al.*, 2001). Olivine in Dhofar 019 is unusually poor in Ni and with lower Ni/Co.

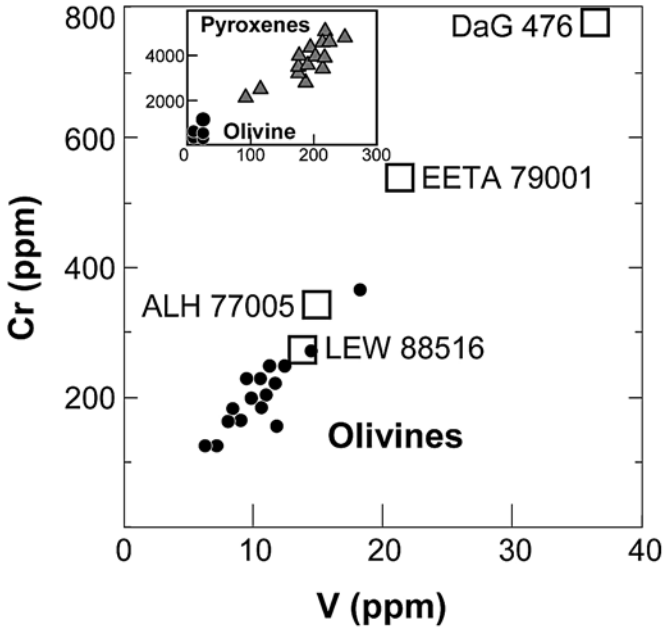

FIG. 8. Contents of Cr *vs.* V for pyroxene and olivine in Dhofar 019. Average compositions of olivine from other martian meteorites are shown (Herd *et al.*, 2001). The Cr and V correlate well in pyroxene and olivine. Olivine in Dhofar 019 is generally lower in V and Cr than that in olivine-bearing basaltic and lherzolitic shergottites.

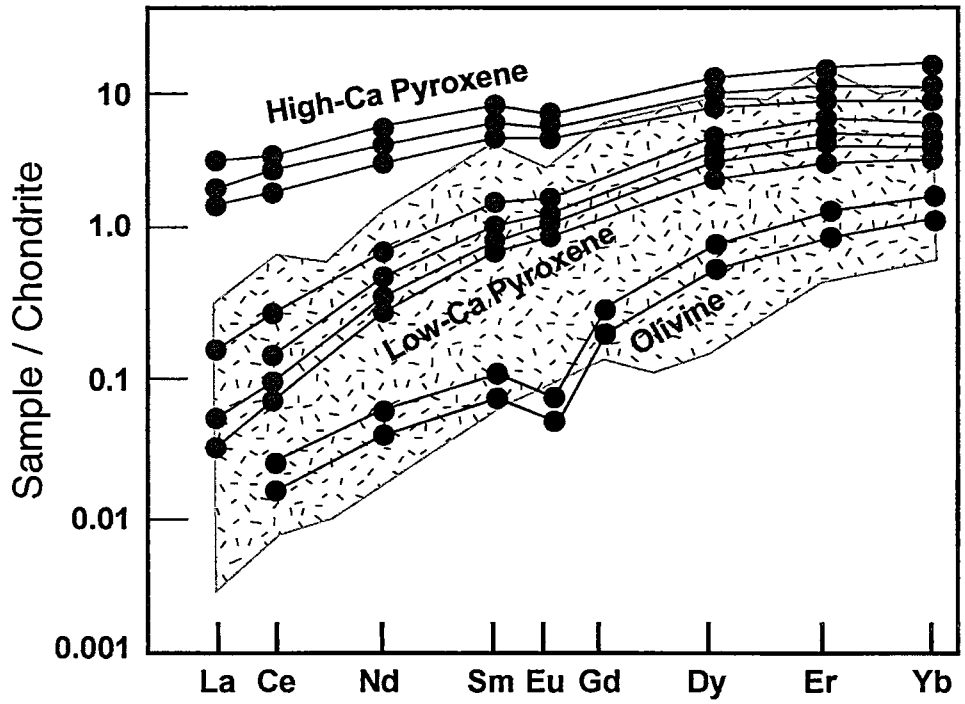

FIG. 9. Patterns of REEs for augites, pigeonites, and olivines in Dhofar 019. Superimposed for comparison is the field for clinopyroxene from lherzolitic shergottites ALHA77005 and LEW 88516 (Wadhwa, 2001). Pyroxenes and olivines in Dhofar 019 are LREE-depleted. Particularly augite appears higher in REEs compared to that of other SNC meteorites.

Olivines in Dhofar 019 are poorer in Ni (160–290 ppm) and slightly richer in Co (200–330) than olivines in other martian basalts (Fig. 7). No distinction was detected in Ni and Co between the megacrysts and smaller olivines, which suggests that these olivines are co-magmatic. The olivine is commonly zoned, with Ni decreasing and Co increasing from core to rim. This is similar to olivines in other martian meteorites, although the overall slope of Ni *vs.* Co is steeper in Dhofar 019. Contents of Cr and V are strongly correlated in olivines from all the martian shergottites (Fig. 8), with the average Cr and V values decreasing in the order DaG 476 ⇒ EETA79001 ⇒ ALHA77005 ⇒ LEW 88516 ⇒ Dhofar 019. The REE pattern for the olivine is extremely low and LREE-depleted (Fig. 9), and REE abundances are extremely low.

Plagioclase

Plagioclase has been transformed to maskelynite. Only a few optically anomalous areas within maskelynite grains were recognized. These areas have diffuse borders, with slight birefringence, as well as a set of poorly visible planar deformation features (PDF). Maskelynite grains rarely possess

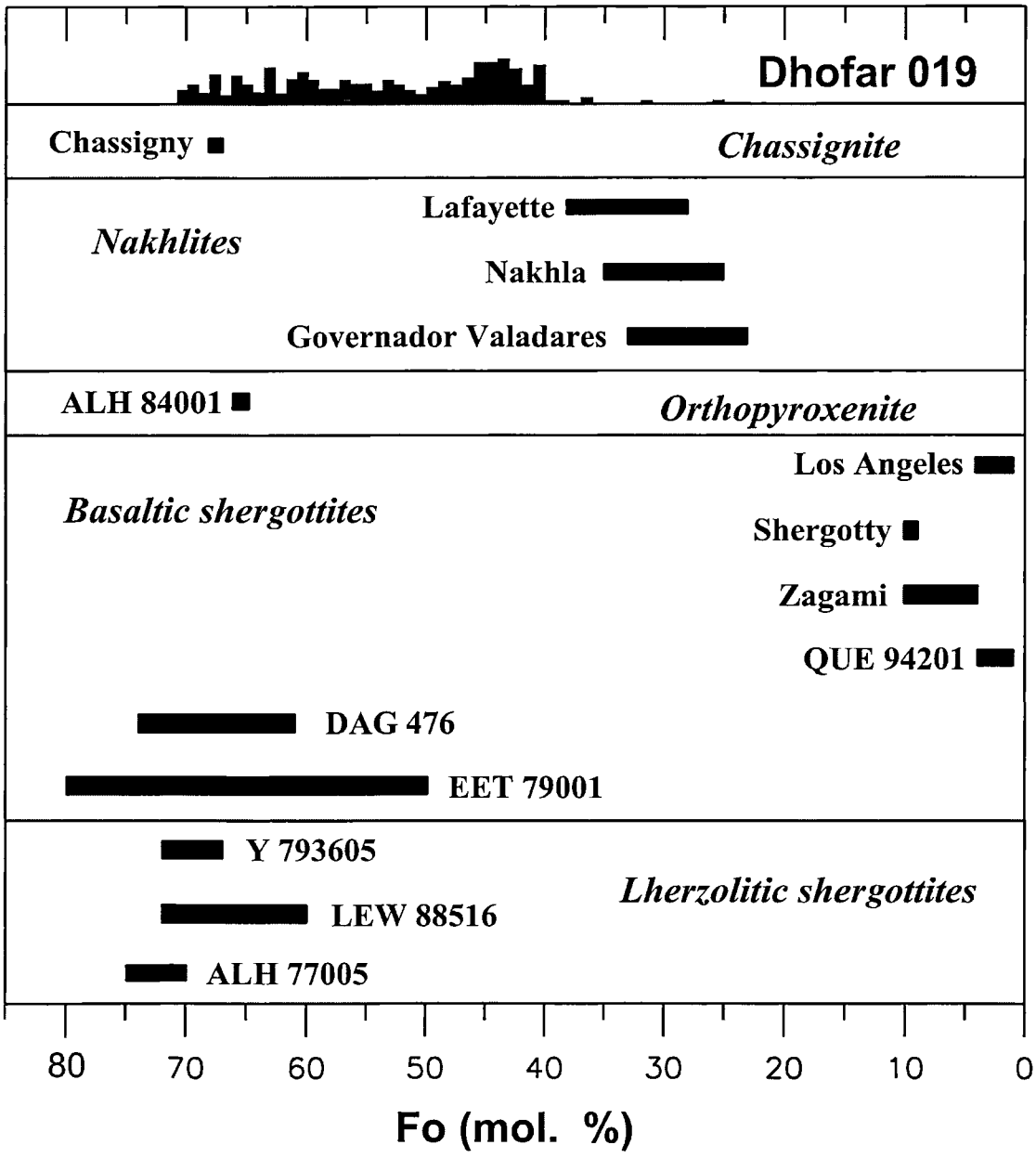

FIG. 10. Olivine compositions in Dhofar 019 and other martian meteorites (Meyer, 1998; Zipfel *et al.*, 2000; Folco *et al.*, 2000; Rubin *et al.*, 2000). Compared to olivines in the SNC suite, most olivines in Dhofar 019 have an intermediate composition.

shock-induced fractures. Such fractures are formed at a shock-wave front, and, therefore, should be destroyed by the compression wave that produced subsequent transformation of plagioclase to diaplectic glass, possibly through a liquid state (Chen and El Goresy, 2000). Besides the presence of maskelynite, Dhofar 019 displays other shock metamorphic features. All olivine grains show moderate to strong mosaicism, whereas pyroxene displays both irregular and planar fractures and undulatory extinction, with slight to moderate mosaicism (Badjukov *et al.*, 2001).

Maskelynite compositions exhibit a large range (An_{86-36}), comparable only to those in the LEW 88516 and ALHA77005 lherzolitic shergottites (Fig. 11). Small maskelynite grains are more variable in composition compared to large ones. The largest grains are commonly zoned from An_{65} cores to An_{50} rims. Rare grains of K-rich feldspar were also analyzed (Table 2), associated with mesostasis. The FeO range in the maskelynite is 0.4–1.0 wt%. These FeO values are similar to those in maskelynite in Shergotty, where Hale *et al.* (1999) proposed that the Fe contents were indicators of oxidizing conditions, supposedly because plagioclase prefers Fe^{3+} as a substitution for Al. However, similar Fe contents are documented in plagioclases in lunar mare basalts (Papike *et al.*, 1991) that were formed under more reducing conditions ($fO_2 < IW$) than SNC rocks. In general, feldspathic

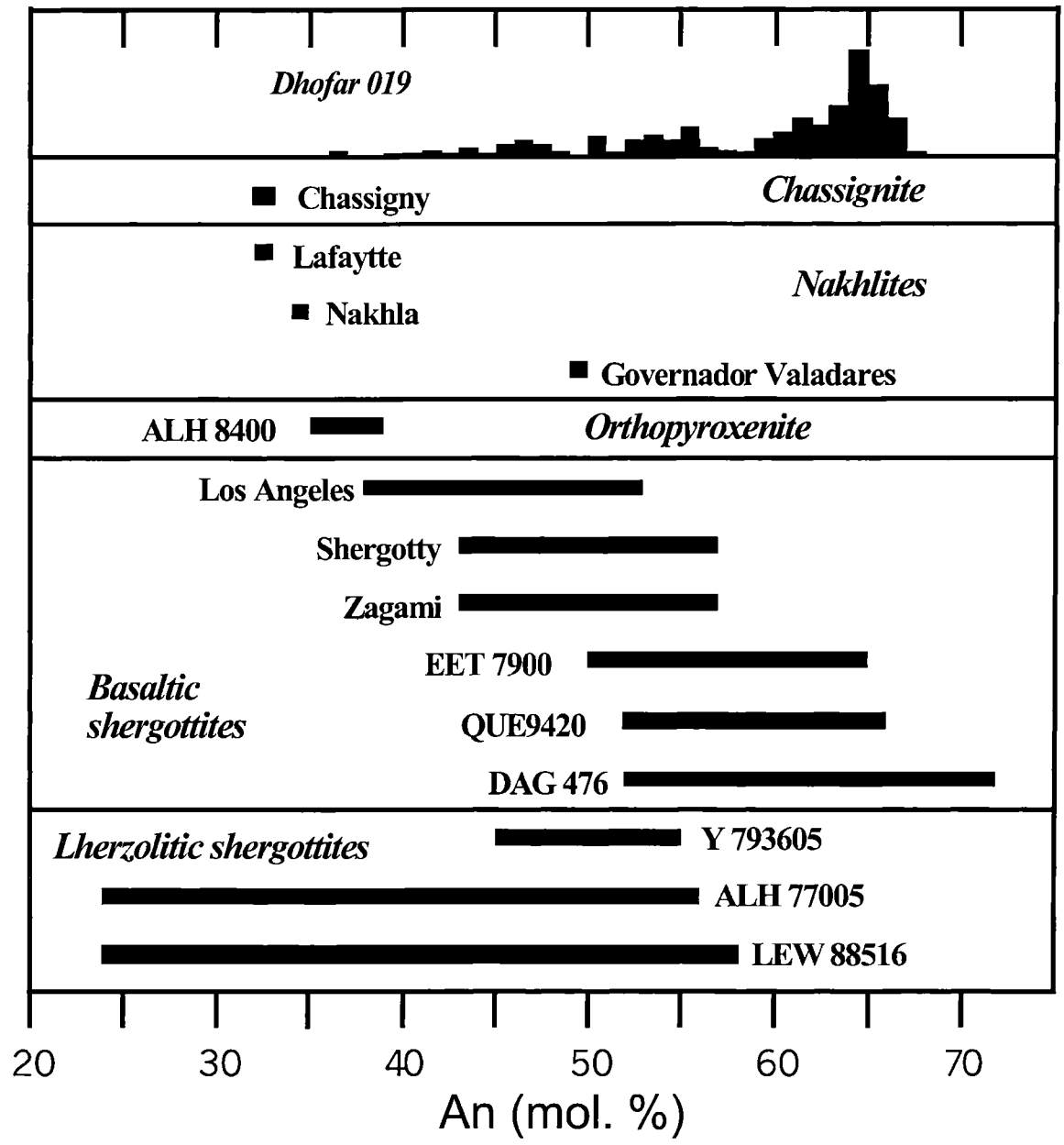

FIG. 11. Compositions of maskelynite/plagioclase in Dhofar 019 and other SNC meteorites (Meyer, 1998; Zipfel *et al.*, 2000; Folco *et al.*, 2000; Rubin *et al.*, 2000). The feldspathic-glass compositions of Dhofar 019 occur over a large range, but in general, are Ca-rich.

glass in Dhofar 019 is richer in CaO (An_{66-58}) relative to other SNC meteorites (Fig. 11), and close in composition to the glass in the QUE 94201 basaltic shergottite and the olivine-bearing basaltic shergottites DaG 476 and EETA79001.

The REE patterns of feldspathic glass exhibit positive Eu anomalies, depletions in HREE, and low Nd/Sm (Fig. 12a). In several analyses, a minor negative Ce anomaly is present in the pattern (Fig. 12b). After examination of ion-probe analytical spots, the anomalous Ce appears to be correlated with terrestrial alteration of the maskelynite, similar to that described by Crozaz and Wadhwa (2001). Compared to the plagioclase component in lherzolitic shergottites LEW 88516 and ALHA77005, the maskelynite in Dhofar 019 has a depleted-LREE pattern. The plagioclase components in basaltic shergottites QUE 94201, EETA79001A, and DaG 476/489 have patterns with similar shapes, with REE abundances that are lower than and overlap those of Dhofar 019 (Fig. 12a).

Spinel Minerals

Spinel minerals in Dhofar 019 vary in composition from chromite to ulvöspinel (Table 2; Figs. 13 and 14a). Cores of spinel crystals consist of chromite to Ti-chromite, which are zoned outward towards the margins with small increases in FeO and TiO_2, and only minor decreases in Cr_2O_3. Some central chromite portions are rimmed by Ti-rich chromite spinel that, in turn, is zoned outward to Cr-ulvöspinel compositions, with large increases in TiO_2 and FeO. However, there is a compositional break between the chromite cores and Ti-chromite/Cr-ulvöspinel rims (Fig. 14a,b), much like in the Apollo 12 lunar basalts (Taylor *et al.*, 1971). Such diversity in spinel compositions has been documented, among martian meteorites, only in EETA79001 and DaG 476/489 (*e.g.*, Folco *et al.*, 2000; Zipfel *et al.*, 2000). Nakhlites and normal basaltic shergottites contain Ti-magnetites, whereas spinels of lherzolitic shergottites and Chassigny are mainly chromites (Fig. 14b).

Ilmenites

Ilmenites of Dhofar 019 contain 1.0–2.5 wt% MgO and 0.4–1.2 wt% Cr_2O_3 (Table 2), with a positive correlation between Mg and Cr. The MgO and Cr_2O_3 contents are similar to those reported in ilmenites in the DaG 476/489 olivine-bearing basaltic shergottites (Zipfel *et al.*, 2000; Folco *et al.*, 2000). The ilmenites are intermediate in Mg and Cr between those in lherzolitic shergottites and basaltic shergottites. No Fe^{3+} was indicated in the ilmenites, based on stoichiometric calculations.

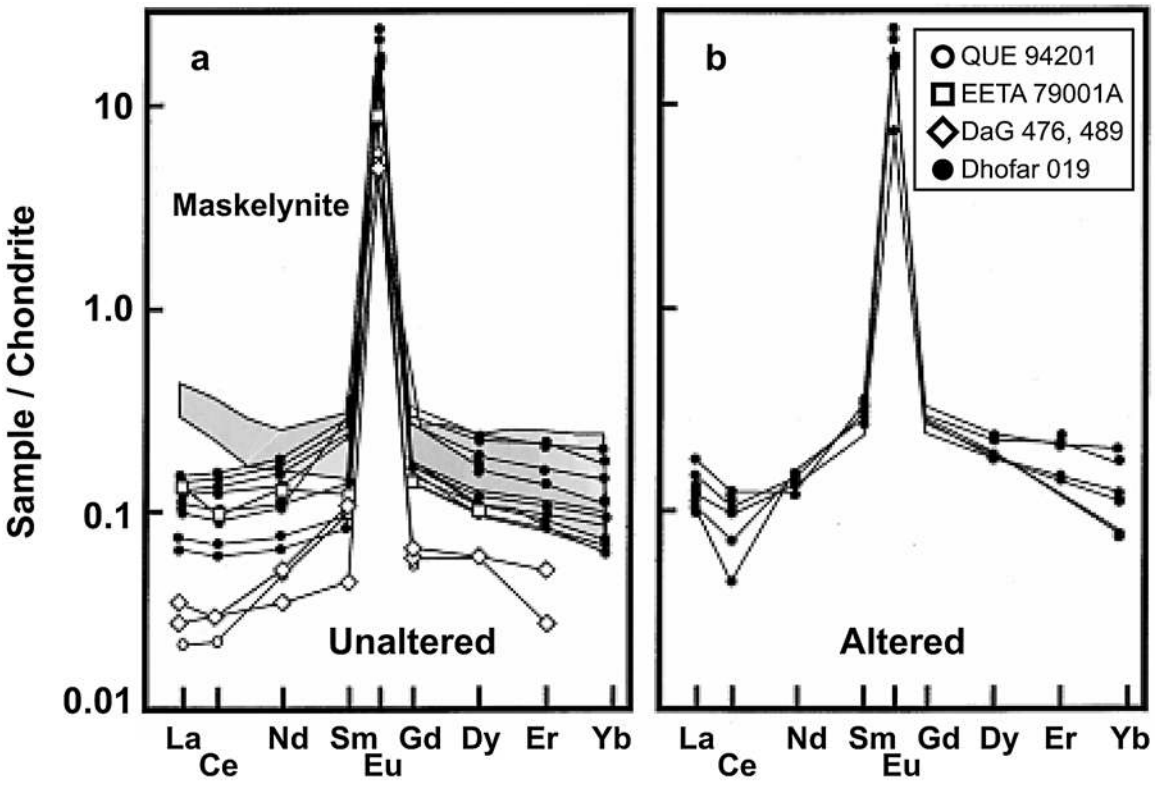

FIG. 12. Patterns of REEs for (a) unaltered and (b) partially altered (terrestrial weathered) feldspathic glass in Dhofar 019. For comparison, superimposed are the field for maskelynite from lherzolitic shergottites and individual analyses of plagioclase from basaltic shergottites (Wadhwa *et al.*, 2001). Maskelynite of Dhofar 019 is LREE-depleted. Notice that several altered maskelynite grains show a small, negative Ce anomaly, possibly from weathering.

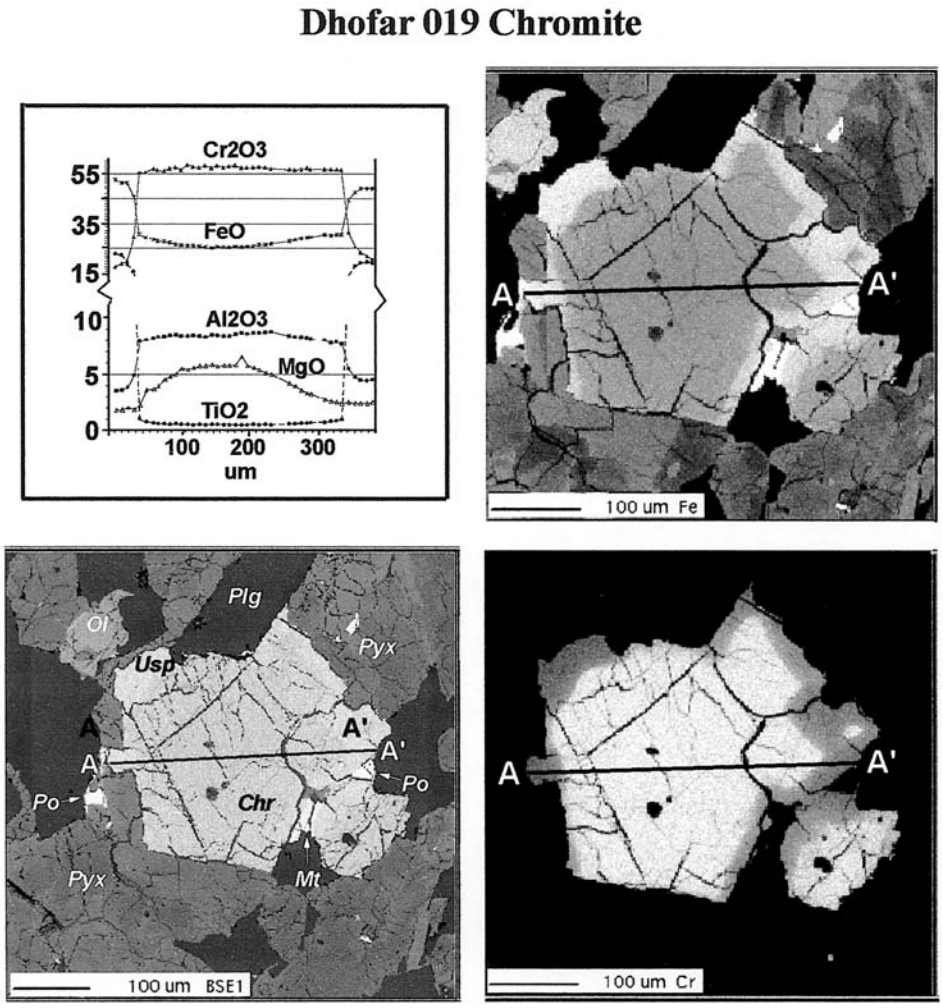

FIG. 13. Elemental maps and compositional profiles of a chromite core with an overgrowth of ulvöspinel, similar to spinel textures in Apollo 12 and 15 mare basalts.

Merrillite (Whitlockite) and Apatite

Both merrillite (whitlockite) and apatite are present in Dhofar 019; however, merrillite is more abundant. The REE pattern of merrillite is LREE-depleted, with La = 40 to 100× chondrites, Nd = 100 to 200× chondrites, and Yb = 200 to 400× chondrites. The merrillite also contains a small negative Eu anomaly. The overall merrillite REE pattern is roughly parallel to those of other basaltic shergottites. However, the merrillite from Dhofar 019 exhibits more variability and REE concentrations overlap or are greater than documented in QUE 94201 and EETA79001A (Wadhwa *et al.*, 2001) and in DaG 476/489 (Crozaz and Wadhwa, 2001).

Pyrrhotite

Pyrrhotite is the only sulfide mineral occurring in Dhofar 019. The range in (Fe + Ni + Co)/S atomic ratios is 0.85–0.93, with an average of 0.875, corresponding to Fe_7S_8 ("monoclinic pyrrhotite"; Taylor, 1970), with Ni contents in the range of 0.25–0.76 wt% and with Co contents up to 0.22 wt%. These concentrations are similar to those reported in sulfides from other SNC meteorites (*e.g.*, Meyer, 1998).

Secondary Phases

Secondary phases analyzed in Dhofar 019 are calcite, gypsum, celestite, and two types of smectite (Table 2). The first is Mg- and Al-rich and compositionally close to montmorillonite. It is most abundant and present in the zoned, near-circular aggregates (Fig. 3c–e). The second is Fe-rich and Al-poor and similar in composition to saponite. This phase is rare and replaces olivine.

To summarize the mineral chemistry of Dhofar 019, its minerals are most similar to the basaltic shergottites DaG 475/489 and EETA79001A. The most notable features of the Dhofar

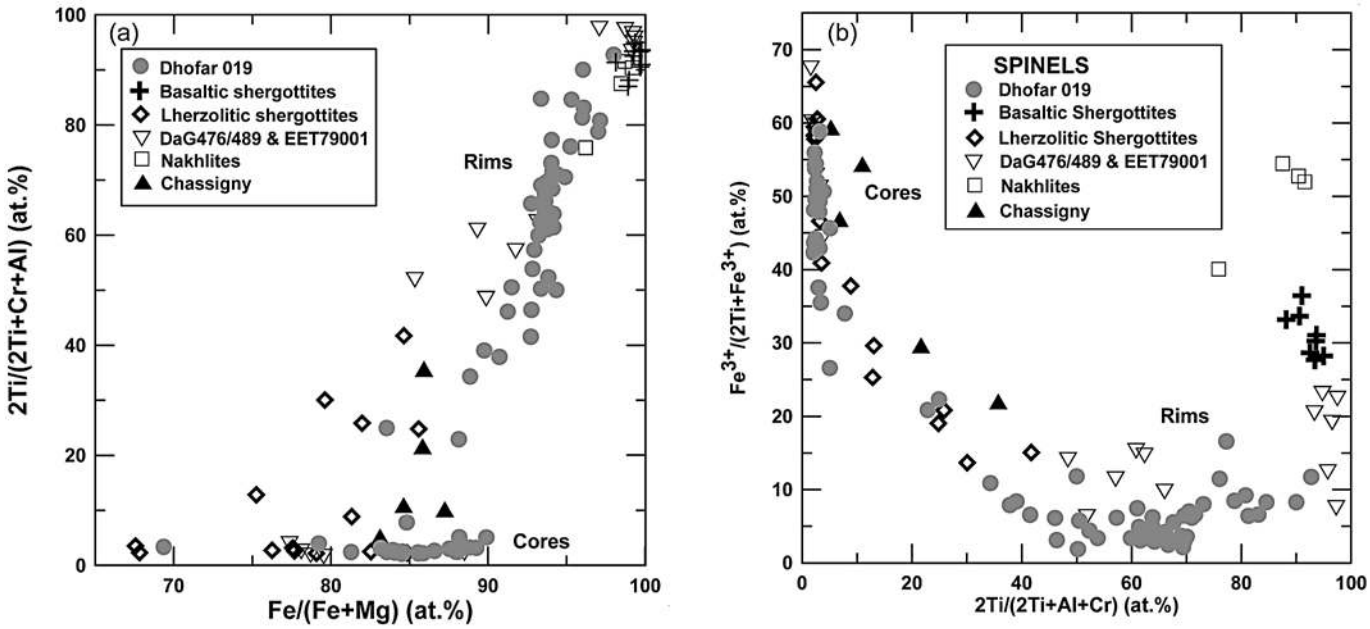

FIG. 14. Compositional variations of spinels in Dhofar 019 and SNC meteorites. (a) 2Ti/(2Ti + Cr + Al) *vs.* Fe/(Fe + Mg). Cores of spinel crystals consist of chromite, which zone outward with small increases in Fe and Al, followed by rims that become increasingly Ti-rich. (b) $Fe^{3+}/(2Ti + Fe^{3+})$ *vs.* 2Ti/(2Ti + Cr + Al). Spinels of Dhofar 019 are generally lower in Fe^{3+} than those in other SNC rocks. Data sources: Floran *et al.* (1978); Folco *et al.* (2000); Hale *et al.* (1999); McSween and Jarosewich (1983); Smith and Hervig (1979); Stolper and McSween (1979); Treiman *et al.* (1994); Zipfel *et al.* (2000).

019 mineral chemistry are the large compositional ranges of the olivine, maskelynite, and spinels, with the modest range of the pyroxenes. Such compositional ranges imply the relatively rapid differential crystallization of the Dhofar 019 melt, probably as a lava flow.

BULK CHEMISTRY AND OXYGEN ISOTOPES

The average major and trace element abundances are given in Table 3. High CaO, SO_3, CO_2 and H_2O contents of Dhofar 019 point to a significant terrestrial enrichment in secondary Ca-carbonates, Ca-sulfates, and clay minerals. The carbonate and sulfate contents are estimated to be ~3 and 2 wt%, respectively. The bulk composition was computed to a $CaCO_3$-$CaSO_4$-, and H_2O-free basis (Table 3); while still containing probable terrestrial alteration phases, this computation is certainly more realistic. However, this calculated composition of the original melt is possibly still enriched in Si, Na, and poorer in Al, from terrestrial contamination. The replacement of feldspar glass by smectite should lead to a loss of Si and Na and enrichment in Al. Thus, Dhofar 019 major element chemistry, given in Table 3, indicates pervasive terrestrial alteration. Petrogenetic conclusions, therefore, must be considered in light of this estimated whole-rock composition, which may differ significantly from that of the pristine rock.

In bulk composition, Dhofar 019 is like the DaG 476/489 and EETA79001A olivine-bearing basaltic shergottites, which are intermediate in chemistry between lherzolitic and basaltic shergottites (Table 3). Compared to the olivine-bearing shergottites, Dhofar 019 is richer in Al and, to a lesser extent, in Fe. The Al and Fe contents of Dhofar 019 are compatible with those in normal basaltic shergottites. In trace element contents, Dhofar 019 is also closer to the olivine-bearing basaltic shergottites (Table 3). However, it is richer in Cr and poorer in incompatible elements relative to normal basaltic shergottites. On the other hand, Dhofar 019 is depleted in compatible elements and enriched in incompatible elements as compared to lherzolitic shergottites. Certain element ratios in Dhofar 019, $Ga_{(ppm)}/Al_{(wt\%)}$ = 2.9, Ni/Co = 1.47, and Ni/Mg = 0.00074, are lower than those of basaltic shergottites. The depletion in Ni is consistent with the unusually low Ni measured in olivine (Fig. 7). The LREEs in Dhofar 019 are strongly depleted, and a weak negative Eu anomaly is probably present. The anomaly is well expressed in the INAA data, but the ICP-MS measurements reveal only a minute Eu depletion (Fig. 15), possibly due to sampling (1 g *vs.* 0.1 g, respectively). This REE pattern is similar to that of EETA79001A and DaG 476/489, but these meteorites do not show Eu depletion. The depletion, if it is a primary feature, is a signature of the reducing conditions during crystallization of Dhofar 019. However, the anomaly could also result from preferential decomposition of feldspar glass during terrestrial weathering, as addressed below.

The PGE contents of Dhofar 019 are similar to EETA79001 (Fig. 16). Such a fractionated pattern is entirely consistent with

TABLE 3. Chemical composition of Dhofar 019 in comparison with other shergottites.

	Vernadsky analyses‡	Notre Dame§	$CaCO_3 + CaSO_4$ free composition#	Basaltic shergottites§	"Ol-bearing" shergottites@	Lherzolitic shergottites¥
SiO_2	45.52	–	48.4	48.0–51.4	45.8–50.6	43.1–45.4
TiO_2	0.594	0.49	0.63	0.73–1.98	0.35–0.70	0.35–0.44
Al_2O_3	6.72	6.65	7.01	5.70–13.4	4.19–5.85	2.32–3.45
Cr_2O_3	0.574	–	0.61	0.01–0.20	0.63–0.83	0.84–1.03
FeO*	17.93	19.9	19.1	17.0–21.4	16.1–18.5	19.7–20.9
MnO	0.461	0.48	0.49	0.41–0.52	0.39–0.49	0.44–0.51
MgO	14.61	14.6	15.5	3.53–9.28	14.6–19.4	23.7–27.7
CaO	9.27	9.42	7.08	10.0–11.5	7.42–7.83	3.35–4.25
Na_2O	0.677	0.89	0.72	1.20–2.17	0.51–0.80	0.35–0.59
K_2O	0.053†	–	0.05	0.04–0.03	0.03–0.04	0.02–0.03
P_2O_5	0.401	0.40	0.41	0.48–1.50	0.32–0.49	–
SO_3	1.15†	–	–	–	–	–
CO_2	1.42†	–	–	–	–	–
H_2O	0.39†	–	–	–	–	–
Total	99.77	–	100.0	–	–	–
Li	–	2.86	–	2.2–5.6	2.6–4.5	1.3–1.6
Be	–	0.03	–	–	–	–
Sc	33.8	31.2	–	43–59	28–37	21–25
V	–	175.1	–	103–380	171–230	132–202
Cr	3900	3417	–	96–1389	4290–5700	5672–6900
Co	39.1	44.5	–	24–51	43–51	63–72
Ni	100	65.3	–	20–83	128–300	250–370
Cu	–	9.54	–	11–139	7–80	5–80
Zn	–	62.0	–	54–130	49–85	47–90
Ga	–	10.21	–	14–30	8–14	6–9
Se	0.32	–	–	0.2–0.5	0.4–0.5	0.04–0.5
Br	0.19	–	–	0.3–1.1	0.2–1.3	0.05–0.08
Rb	–	0.49	–	0.1–14	0.9–6.9	0.17
Sr	285†	363†	–	35–80	40–87	8–30
Y	–	6.78	–	10–28	8	5.7–6.2
Zr	50	17.4	–	41–97	8–90	10–19
Nb	–	0.30	–	0.7–22	0.13	0.5–0.6
Mo	–	0.52	–	0.37	0.18	47.3
Ru	–	0.354	–	–	–	–
Rh	–	0.295	–	–	–	–
Pd	–	1.718	–	–	–	–
Sb	40†	–	–	2–27	10	0.7–2
Cs	0.32	0.03	–	0.3–0.7	0.07–0.6	0.03–0.08
Ba	70†	19.4	–	25–80	<48	2.3–6
La	0.3	0.24	–	0.4–5.3	0.1–0.5	0.2–0.3
Ce	1.1	1.45†	–	1.6–13	0.4–1.7	0.9–1.1
Pr	–	0.11	–	0.7–0.9	–	0.13
Nd	1.6	0.69	–	2.4–11	0.6–1.2	0.8–1.1
Sm	0.82	0.48	–	1.2–3.4	0.4–0.8	0.3–0.4
Eu	0.14	0.20	–	0.5–1.2	0.2–0.4	0.1–0.2
Gd	–	0.99	–	1.6–4.3	1.00	0.4–1.1
Tb	0.22	0.20	–	0.4–0.9	0.2–0.3	0.1–0.2
Dy	–	1.30	–	1.7–6.1	1.4–2.2	0.6–1.3
Ho	–	0.27	–	0.6–1.3	0.3–0.5	0.2–0.3
Er	–	0.81	–	–	0.9	0.3–0.7
Tm	–	0.12	–	0.2–0.4	0.1–0.2	0.08–0.12
Yb	0.74	0.81	–	1.4–3.5	0.8–1.2	0.4–0.5
Lu	0.13	0.12	–	0.2–0.5	0.1–0.2	0.06–0.08
Hf	0.7	0.48	–	1.9–3.4	0.4–1.0	0.4–0.6
Ta	0.1	0.02	–	0.02–0.4	0.01–0.03	0.02–0.04

TABLE 3. *Continued.*

	Vernadsky analyses‡	Notre Dame§	$CaCO_3$ + $CaSO_4$ free composition#	Basaltic shergottites$	"Ol-bearing" shergottites@	Lherzolitic shergottites¥
W	–	30	–	160–500	0.08–240	38–250
Ir	<9	0.127	–	0.03–0.4	<6	1.6–9.1
Pt	–	3.969	–	–	–	–
Pb	–	0.92	–	–	<0.04	–
Th	–	0.04	–	0.05–0.9	0.02–1.0	0.04–0.06
U	–	0.11†	–	0.01–0.17	0.02–0.6	0.01–0.04

Major elements in wt%, Sb, W, Ir, Ru, Rh, Pt; Pd in ng/g; all others in μg/g.
*Total Fe as FeO; the bulk Dhofar 019 contains 0.94 Fe_2O_3 and 17.08 FeO (wt%).
†Suspected to be due to terrestrial weathering.
‡Major elements from inductively coupled plasma and x-ray flourescence spectroscopy, Na and K from atomic absorption, C and S from a combustion analyzer, trace elements from instumental neutron activation analysis.
§The data are from inductively coupled plasma-mass spectroscopy.
#Carbonate- and sulfate-free basis computed from column 1.
$The ranges are for Shergotty, Zagami, Los Angeles, Queen Alexandra Range 94201, Elephant Moraine (EET) A79001B (Meyer, 1998; Warren *et al.*, 2000).
@The ranges are for Dar al Gani (DaG) 476, DaG 489, and EETA79001A, not olivine-bearing *sensu stricto* (Meyer, 1998; Zipfel *et al.*, 2000; Folco *et al.*, 2000).
¥The ranges are for Lewis Cliff 88516, Allan Hills A77005, Yamato-793605 (Meyer, 1998).

the mineral and rock REE contents (Figs. 9–12, 15 and 16). Therefore, Dhofar 019 seems to represent a melt derived from a source already depleted in the incompatible elements and PGEs. This is consistent with isotopic data for this martian meteorite (Borg *et al.*, 2001).

Numerous elemental ratios of Dhofar 019 are in the range of those in other SNC meteorites (*e.g.*, Treiman *et al.*, 1986; Zipfel *et al.*, 2000): Fe/Mn = 39, Na/Al = 0.20, Na/Ti = 1.62, P/Ti = 0.49, and $Co_{(ppm)}/(MgO + FeO)_{(wt\%)}$ = 1.20. The high K/La (1470) of Dhofar 019 can be attributed to terrestrial weathering (Zipfel *et al.*, 2000; Crozaz and Wadhwa, 2001). The enriched U contents (relative to Th) and a small positive Ce anomaly (Fig. 15) could also be terrestrial weathering artifacts. It would appear anomalous in a rock to have both a negative Eu anomaly (indicating reducing conditions for Eu^{2+} formation) and a positive Ce anomaly (indicating oxidizing conditions for Ce^{4+} formation). However, the source of the negative Eu anomaly is inherited from the primary igneous minerals, whereas the presence of Fe hydroxides as weathering products may be the focus of elevated Ce in the 4+ state. It has been demonstrated that under oxidizing conditions, Ce^{4+} is scavenged by Fe-rich minerals (*e.g.*, Fleet, 1984). Note that the REE composition for Dhofar 019 measured by INAA (Table 3) did not exhibit the positive Ce anomaly. This may indicate that the INAA analyzed aliquot contained a lower proportion of secondary Fe-hydroxide minerals. The higher proportion of these minerals in the ICP-MS analyzed aliquot may be indicated by its higher Fe contents (Table 3). Contents of Sr, Sb, and Ba (Table 3) may also be affected by the terrestrial weathering (*e.g.*, celestite has been observed in the alteration of this meteorite).

Oxygen Isotope Measurements

Oxygen isotope measurements (Fig. 17) indicate that Dhofar 019 has the highest $\delta^{17}O$ (2.99‰) and $\delta^{18}O$ (5.40‰) among the martian meteorite suite (Clayton and Mayeda, 1996; Franchi *et al.*, 1999). The $\Delta^{17}O$ value of Dhofar 019 is 0.18, placing it relatively close to the terrestrial fractionation line, thereby providing additional evidence for the presence of terrestrial weathering products.

CRYSTALLIZATION HISTORY

Age of Crystallization

In order to obtain a reliable age for Dhofar 019, removal of the secondary alteration products was required. Based upon extensive leachings and mineral separations of Dhofar 019, Borg *et al.* (2001) determined an Sm-Nd age of 586 ± 9 Ma, with an initial ϵ_{Nd} value of +34.6 ± 0.6, as defined by the silicate-mineral fractions, whole rock, and leachates. Although the Rb-Sr isotopic systematics of Dhofar have been disturbed by terrestrial weathering, an age of 525 ± 56 Ma was derived from the least-altered mineral fractions. Most coarse-grained mineral fractions, as well as the leachates, fall significantly above the best Rb-Sr isochron as a result of the presence of secondary alteration products with $^{87}Sr/^{86}Sr$ ratios near modern seawater. The maximum initial $^{87}Sr/^{86}Sr$ ratio of Dhofar 019 determined from this isochron is 0.70215 ± 3.

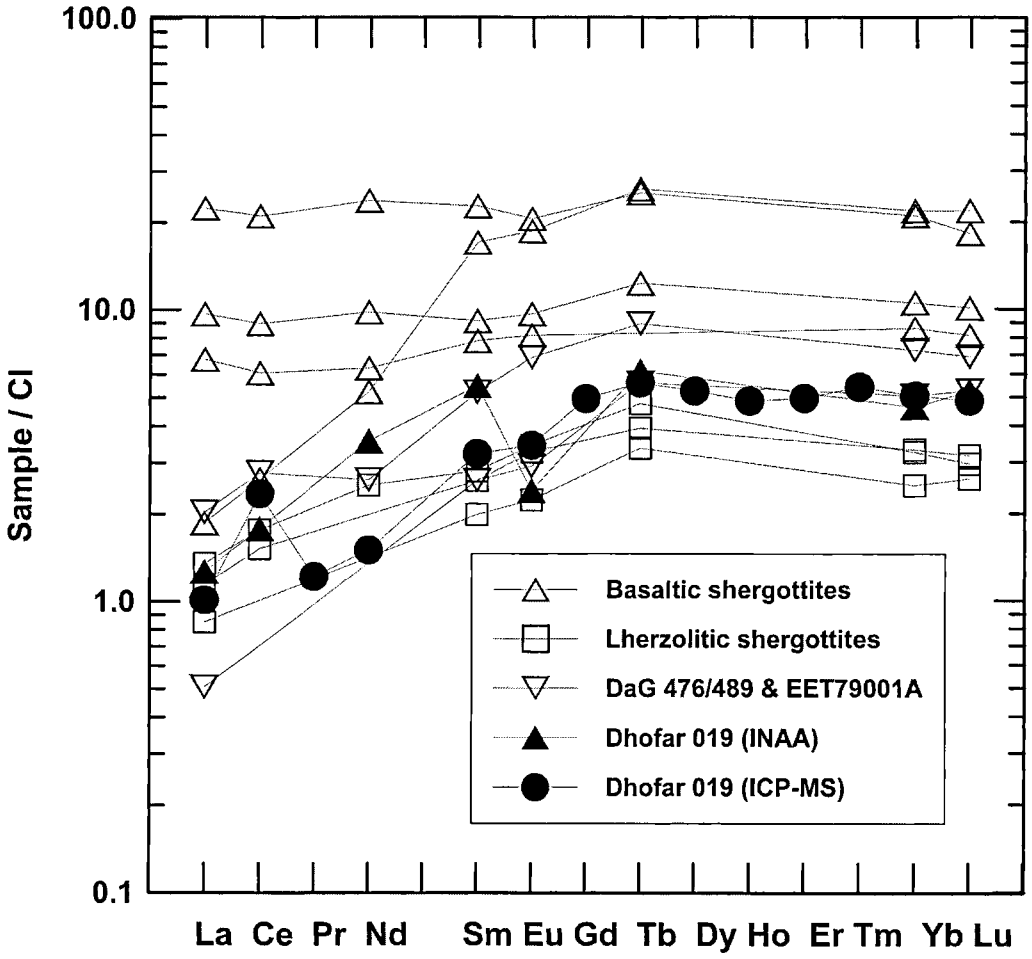

FIG. 15. Patterns of REEs for bulk-rock Dhofar 019 and shergottites (Meyer, 1998; Zipfel *et al.*, 2000; Folco *et al.*, 2000). Similar to lherzolitic shergottites, DaG 476/489, EETA79001A, EETA79001B, QUE 94201, and Dhofar 019 shows strong LREE depletion. A negative Eu anomaly is possibly present in Dhofar 019; because of the differences in Eu-REE patterns from two analytical techniques used, this Eu anomaly is suspect.

Redox Conditions

The spinels of Dhofar 019 contain some Fe^{3+}, but the amount calculated by stoichiometry is <10% of the Fe present and does not differ significantly in Ti-poor chromites and ulvöspinels. A computed $Fe^{3+}/(2Ti + Fe^{3+})$ atomic ratio (*i.e.*, the magnetite component in magnetite-ulvöspinel) is highest in Ti-poor chromite. This ratio appears to have decreased during crystallization, but has increased slightly again in the late-crystallized ulvöspinel (Fig. 14b). This ratio in the Ti-poor chromites of other SNC meteorites are similar to those of Dhofar 019, but the ratios in Ti-rich chromites and ulvöspinels of Dhofar 019 are generally lower than those of other SNC rocks (Fig. 14b). This suggests that late-stage crystallization took place under more reducing conditions compared to other SNC melts.

The ilmenite and spinel compositions deviate significantly from the ideal Fe-Ti end-members for which oxygen barometers

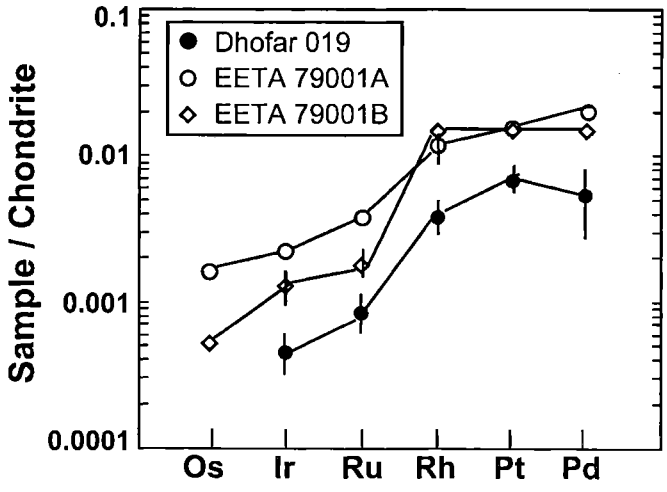

FIG. 16. The pattern for PGEs for bulk-rock Dhofar 019 and EETA79001 shergottites.

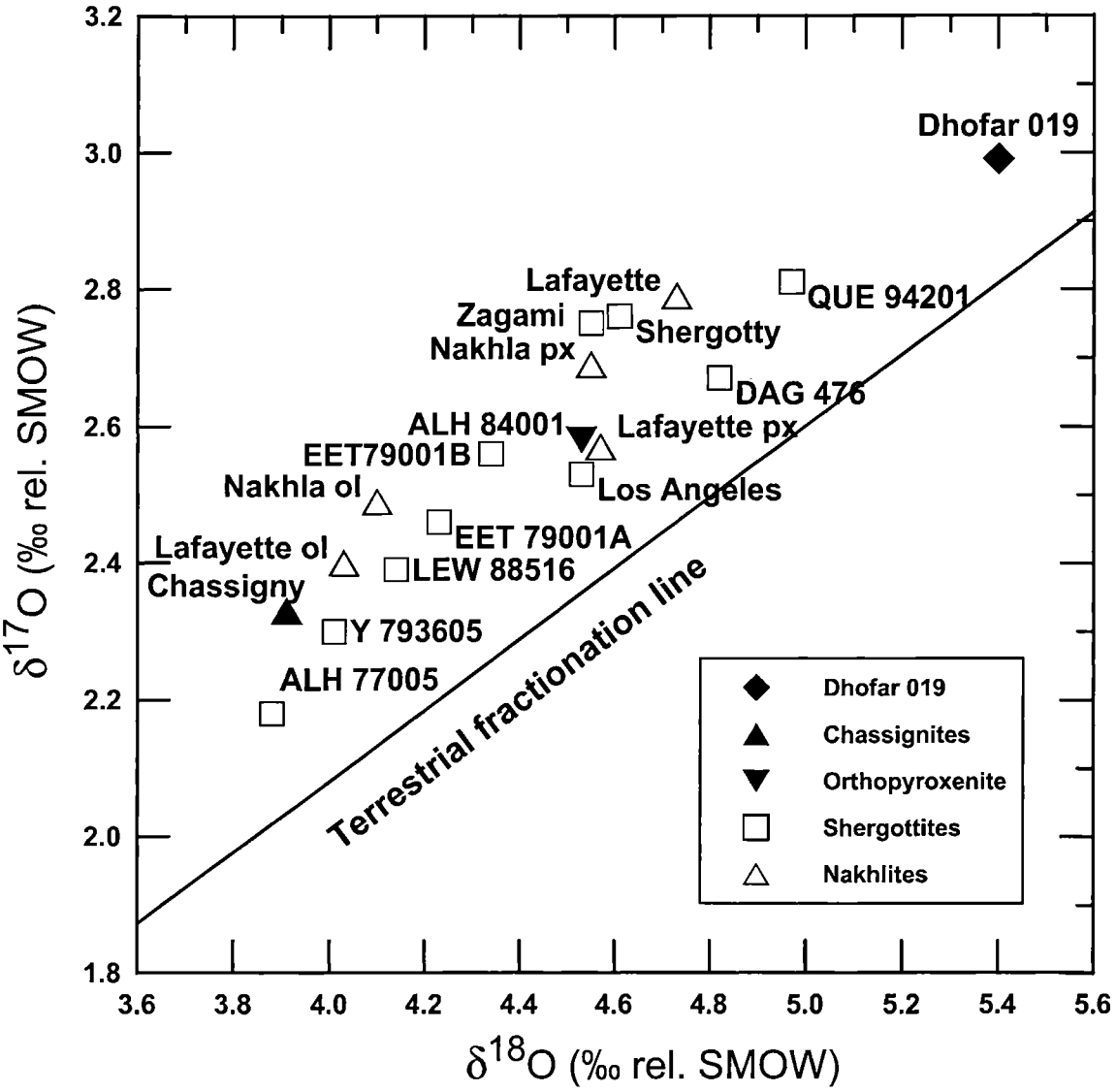

FIG. 17. Oxygen-isotopic composition of Dhofar 019 and martian meteorites (Clayton and Mayeda, 1996). Of all the martian meteorites, Dhofar 019 is the most enriched in $\delta^{17}O$ and $\delta^{18}O$. This depletion in ^{16}O is probably due to terrestrial weathering.

have been developed. Applying the Ghiorso and Sack (1991) oxybarometer/thermometer to these oxide pairs results in subsolidus temperatures of 650–800 °C and fO_2 values that are 3.8–4.3 log units below the QFM buffer. This translates into an fO_2 of ~3 log units below the QFM buffer at 1200 °C, just above the iron/wüstite buffer curve. This value is significantly more reducing that most SNC meteorites (Herd *et al.*, 2001), but is in keeping with the low Fe^{3+} contents.

Crystallization Relationships

Crystallization was modeled at an fO_2 of QFM –3 log units and 1 atmosphere total pressure using the MELTS program of Ghiorso and Sack (1995) (Fig. 18). MELTS was specifically calibrated relative to experimental data on the crystallization of SNC melts (Stolper and McSween, 1979; Longhi and Pan, 1989; McCoy and Lofgren, 1999).

Our model calculations (Fig. 18) reveal that the Dhofar 019 melt, having the composition approximated from the bulk rock, minus the CO_2, SO_3, and H_2O terrestrial contribution (Table 3), is not multiply saturated with respect to the silicate minerals. The order of appearance of phases during equilibrium crystallization (Fig. 18) is olivine + spinel ⇒ orthopyroxene ⇒ pigeonite ⇒ plagioclase ⇒ augite. About 10–12% crystallization of olivine and spinel is required before orthopyroxene appears. Olivine then reacts with the melt, decreasing in abundance. The computed sequence is not compatible with that inferred from the mineralogy and texture of the rock in that no orthopyroxene has been found in detailed examination of four thin sections. Although the model does adequately reproduce the early-formed

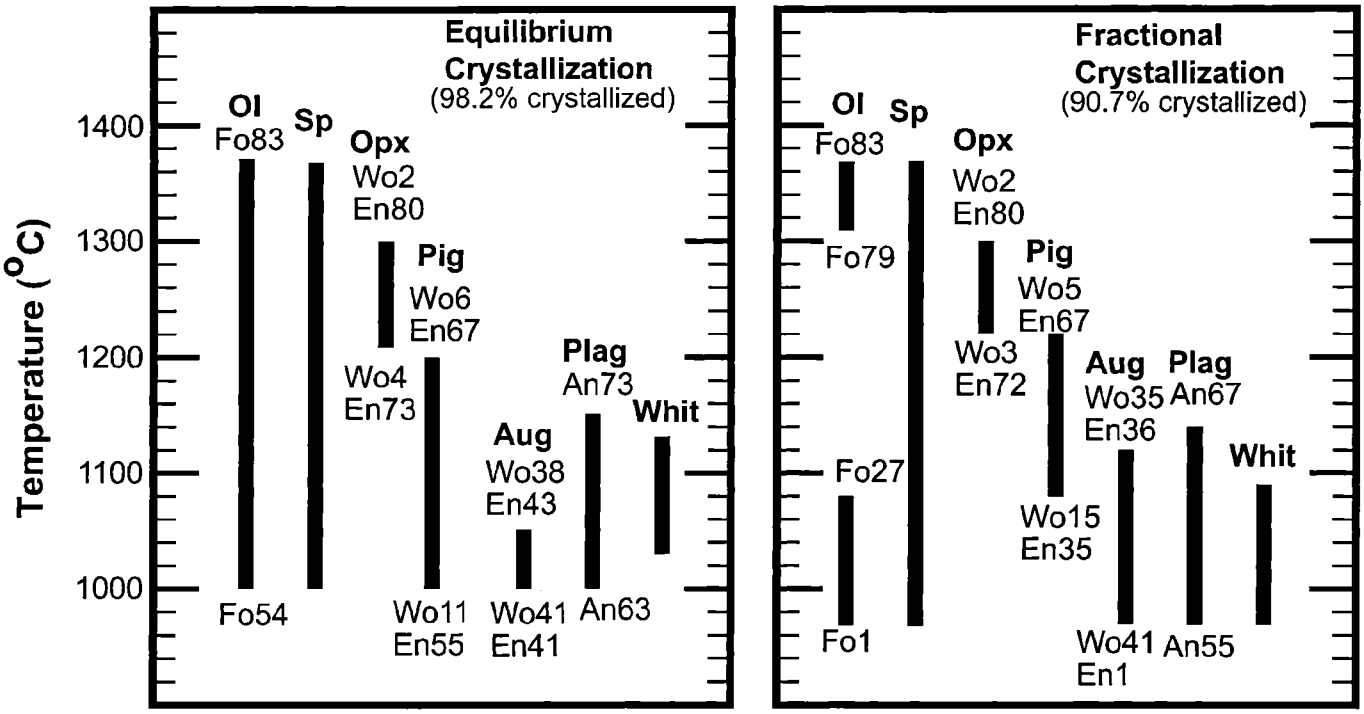

FIG. 18. Modeling of the crystallization of the Dhofar 019 melt at an fO_2 = –3 log units below QFM. This modeling used the MELTS program of Ghiorso and Sack (1993) and the bulk composition in the third column of Table 3 (*i.e.*, measured bulk minus ($CaCO_3$ + $CaSO_4$ + H_2O)). Note the presence of orthopyroxene in the crystallization model, a phase not found in Dhofar 019.

plagioclase and pyroxene compositions, the computed olivine compositions are generally richer in Mg/Fe compared to those observed in the rock.

Fractional crystallization (Fig. 18) gives a better correspondence between the modeled and the observed compositions of feldspar and pyroxenes. This suggests that some fractionation resulted from isolation of growing crystals and restriction of diffusive exchange during cooling and crystallization of the Dhofar 019 melt, a plausible scenario for a basalt. The abundances of augite and the occurrence of merrillite (whitlockite), as calculated from the MELTS program, are close to that observed in the rock. Once again, the lack of orthopyroxene in the rock contrasts with the modeling results.

Even subtracting some of the high-Fo olivine from the bulk-rock composition (on the assumption that it is cumulate) does not significantly change the mineral chemistry or sequence of crystallization of the models. Our modeling with –5% olivine does not significantly modify mineral sequences, compositions, or abundances. (This idea has been used to explain the origin of olivine megacrysts in EETA79001A and DaG 476/489 (*e.g.*, Wadhwa *et al.* 2001).) Thus, we do not put too much significance on the model calculations, because of the uncertainty of the whole-rock composition due to the carbonate and sulfate weathering products. In addition, opal and various forms of silica are found on many of the desert meteorites. Even a few extra percent of terrestrial SiO_2 would significantly affect the modeling.

Olivine Cooling Rates

Zoning in olivine megacrysts can be used to estimate a lower limit to their cooling rate (Taylor *et al.*, 1977, 1978; Onorato *et al.*, 1978). That is, they must have cooled at a rate fast enough to maintain the observed zonation; if slower, the zonation would have been homogenized by diffusion. At slow cooling rates, a primary compositional gradient will tend to decrease with time.

The compositional ranges within olivine megacrysts in Dhofar 019 are typically <20% Fo. The intra-diffusional coefficients for Fe and Mg in olivine are a function of temperature, fO_2, bulk composition of the olivine, and crystallographic direction. The intra-diffusion coefficients used in these estimates are those of Buening and Buseck (1973). A detailed kinetic model developed by Taylor *et al.* (1977) and expanded by Onorato *et al.* (1978) was successfully applied to lunar basalts and meteorites (Taylor *et al.*, 1978). This model starts with assumptions of (a) the temperature at which crystallization begins (1300 °C, in this case); (b) the chemical zoning profile as developed by simple growth of the olivine; (c) diffusion which proceeds during growth of successive zones of the olivine; and (d) an "as-solidified profile" at the solidus of the rock, as a function of the first three factors.

Fe-Mg zoning profiles of olivine megacrysts in Dhofar 019 were analyzed using the kinetic model described and applied by Taylor *et al.* (1978). An fO_2 of QFM –3 log units was

assumed, and anisotropic diffusion rates were considered for modeling of the zoning profiles. Minimum cooling-rate estimates for the Dhofar 019 megacrysts are 0.5–0.8 °C/h. Such cooling rates are generally possible for the center of a thick (*e.g.*, 20–30 m) lava flow, or in a shallow intrusion.

Relations to Other Shergottites–Nakhlites–Chassigny Group Meteorites

Possible relatives of Dhofar 019 are the lherzolitic and olivine-bearing shergottites, all of which contain olivine as a liquidus phase, whereas other basaltic shergottites do not have liquidus olivine. Therefore, equilibrium phase relations computed for such olivine-bearing rocks, at an fO_2 of QFM and 1 atmosphere total pressure using the MELTS program (Ghiorso and Sack, 1995), are generally similar to those of Dhofar 019, except they do not have the predicted presence of orthopyroxene. Their melt compositions on the low-Ca pyroxene-olivine liquidus boundary are given in Table 4. The calculated compositions of pyroxenes on the boundary are close to those of early-formed pyroxenes observed in the rocks. Thus, Dhofar 019 and other olivine-bearing shergottites may be derived mainly by olivine accumulation from their parent melts, which should be higher in olivine content relative to their low-Ca pyroxene-olivine co-saturated melts. Interestingly, such parental melts have similar bulk compositions, as well as olivine and low-Ca pyroxene compositions equilibrated with the melts (Table 4). These rocks were formed from compositionally similar parent melts derived from LREE-depleted sources. Their bulk compositions may have been controlled significantly by olivine accumulation. All these considerations can be taken to indicate that lherzolitic and olivine-bearing shergottites, as a group, could have formed from a chemically similar source(s) and parent melt(s).

SUMMARY

In texture, mineral chemistry, and major and trace element contents, Dhofar 019 can be classified as an olivine-bearing basaltic shergottite. This meteorite is most similar to the EETA79001A and DaG 476/489 shergottites. The main features that distinguish Dhofar 019 from the shergottites and other known SNC meteorites are the lack of orthopyroxene; the lower Ni and higher Co content of olivine; and the heavy oxygen isotopic composition. This last characteristic may have been affected by terrestrial weathering. Dhofar 019 contains abundant secondary phases (calcite, gypsum, celestite, Fe hydroxides, smectite) of terrestrial origin, with the possible exception of some of the smectite. The terrestrial alteration affected the chemical and isotopic characteristics of the meteorite.

When compared to other SNC meteorites, Dhofar 019 displays large compositional ranges for olivine, maskelynite, and spinel, probably a result of the relatively rapid cooling rate of the melt (0.5–0.8 °C/h). The age of crystallization was determined as 589 ± 6 Ma (Borg *et al.*, 2001). Spinel chemistry suggests that crystallization occurred under fO_2 reducing conditions among the lowest estimated for SNC meteorites. This rock has undergone a relatively low-shock loading (<30–35 GPa), shown by the presence of maskelynite.

Olivine megacrysts in Dhofar 019 occur in a range of sizes, but CSD analysis indicates they comprise a single population. However, a few grains of olivine may be cumulates. Lherzolitic shergottites, EETA79001A, DaG 476/489, and Dhofar 019 comprise a magmatic suite of martian rocks, the bulk compositions of which may have been controlled significantly by olivine accumulation. Such rocks could have formed from a chemically similar source(s) and parent melt(s).

TABLE 4. Calculated compositions (wt%) of olivine-pyroxene co-saturated melts of some SNC meteorites.

	Lewis Cliff 88516	Allan Hills A77005	Yamato-793605	Dar al Gani 476	Elephant Moraine A79001A	Dhofar 019
SiO_2	51.8	52.3	53.0	54.1	53.1	53.1
TiO_2	0.70	1.12	0.70	0.60	0.82	0.88
Al_2O_3	6.92	6.88	4.78	6.88	6.92	8.17
FeO	21.3	20.3	21.4	17.9	18.8	18.4
MnO	0.51	0.43	0.51	0.49	0.49	0.48
MgO	9.30	9.32	10.8	10.7	10.1	8.48
CaO	8.21	8.39	8.04	8.45	8.72	9.22
Na_2O	1.18	1.17	0.72	0.81	0.94	1.18
K_2O	0.06	0.08	0.04	0.06	0.05	0.13
Fo*	76	77	79	82	80	77
En†	74	76	76	79	77	71
Fs†	23	22	22	19	20	22

*Olivine compositions (mol%) in equilibrium with the melts.
†Pyroxene compositions (mol%) in equilibrium with the melts.

Acknowledgments–We wish to acknowledge the NASA-sponsored Joint United States/Russia Research in Space Sciences (JURRISS) Program for its support of our Russian colleagues (NAG 5-8726 to L. A. T.). The support of laboratories at the Vernadsky Institute by the Russian Academy of Sciences is also acknowledged. We thank Dawn Taylor for handling figures and Allan Patchen for his assistance with electron microprobe analyses. David Draper and John Jones provided constructive reviews, and Duck Mittlefehldt provided extensive comments and editorial review, and unselfish assistance. Portions of the research have been supported by NASA Cosmochemistry grants to L. A. T., C. .K. S., H. Y. M., C. R. N., and R. N. C., for which we are collectively grateful.

Editorial handling: D. W. Mittlefehldt

REFERENCES

BADJUKOV D. D., NAZAROV M. A. AND TAYLOR L. A. (2001) Shock metamorphism in the shergottite meteorite Dhofar D19 (abstract). *Lunar Planet. Sci.* **32**, #2195, Lunar and Planetary Institute, Houston, Texas, USA (CD-ROM).

BORG L. E., NYQUIST L. E., REESE Y., WIESMANN H., SHIH C-Y., TAYLOR L. A. AND IVANOVA M. (2001) The age of Dhofar 019 and its relationship to the other martian meteorites (abstract). *Lunar Planet. Sci.* **32**, #1144, Lunar and Planetary Institute, Houston, Texas, USA (CD-ROM).

BUENING D. K. AND BUSECK P. R. (1973) Fe-Mg lattice diffusion in olivine. *J. Geophys. Res.* **78**, 6852–6862.

CAHILL J., TAYLOR L. A., PATCHEN A., NAZAROV M. A., STOCKSTILL K. R. AND ANAND M. (2002) Basaltic shergottite Dhofar 019: A "normal" olivine cumulate product (abstract). *Lunar Planet. Sci.* **33**, #1722, Lunar and Planetary Institute, Houston, Texas, USA (CD-ROM).

CHEN M. AND EL GORESY A. (2000) The nature of maskelynite in shocked meteorites: Not diaplectic glass but a glass quenched from shock-induced dense melt at high pressures. *Earth Planet. Sci. Lett.* **179**, 498–502.

CLAYTON R. N. AND MAYEDA T. K. (1983) Oxygen isotopes in eucrites, shergottites, nakhlites and chassignites. *Earth Planet. Sci. Lett.* **62**, 1–6.

CLAYTON R. N. AND MAYEDA T. K. (1996) Oxygen isotope studies of achondrites. *Geochim. Cosmochim. Acta* **60**, 1999–2017.

CROZAZ G. AND WADHWA M. (2001) The terrestrial alteration of Saharan shergottites Dar al Gani 476 and 489: A case study of weathering in a hot desert environment. *Geochim. Cosmochim. Acta* **65**, 971–977.

ELY J. C., NEAL C. R., O'NEILL J. A. AND JAIN J. C. (1999) Quantifying the platinum group elements (PGEs) and gold in geological samples using cation exchange pretreatment and ultrasonic nebulization inductively coupled plasma-mass spectrometry (USN-ICP-MS). *Chem. Geol.* **157**, 219–234.

FLEET A. J. (1984) Aqueous and sedimentary geochemistry of the rare earth elements. In *Rare Earth Element Geochemistry* (ed. P. Henderson), pp. 343–373. Elsevier Sciences Pubs., Amsterdam, The Netherlands.

FLORAN R. J., PRINZ M., HLAVA P. F., KEIL K., NEHRU C. E. AND HINTHORNE J. R. (1978) The Chassigny meteorite: A cumulate dunite with hydrous amphibole-bearing melt inclusions. *Geochim. Cosmochim. Acta* **42**, 1213–1229.

FOLCO L., FRANCHI I. A., D'ORAZIO M., ROCCHI S. AND SCHULTZ L. (2000) A new martian meteorite from the Sahara: The shergottite Dar al Gani 489. *Meteorit. Planet. Sci.* **35**, 827–839.

FOLK R. L. AND TAYLOR L. A. (2000) Nanobacteria on altered pyroxenes in the martian meteorite: Not "Au-artifacts on cleavage", nor "too small for life" (abstract). *Geol. Soc. Am.* **32**, A241.

FOLK R. L., TAYLOR L. A. AND NAZAROV M. A. (2001) Similarity of nanometer-size spheroids in martian meteorite Dhofar 019 and enclosing caliche soil: South-pole *vs.* desert forms (abstract). *Lunar Planet. Sci.* **32**, #1777, Lunar and Planetary Institute, Houston, Texas, USA (CD-ROM).

FRANCHI I. A., WRIGHT I. P., SEXTON A. S. AND PILLINGER C. T. (1999) The oxygen-isotopic composition of Earth and Mars. *Meteorit. Planet. Sci.* **34**, 657–661.

GHIORSO M. AND SACK R. O. (1991) Fe-Ti oxide geothermometry: Thermdynamic formulation and the estimation of intensive variables in silicic magmas. *Contrib. Mineral. Petrol.* **108**, 485–510.

GHIORSO M. AND SACK R. O. (1995) Chemical mass transfer in magmatic processes. IV. A revised and internally consistent thermodynamic model for the interpolation and extrapolation of liquid-solid equilibria in magmatic systems at elevated temperatures and pressures. *Contrib. Mineral. Petrol.* **119**, 197–212.

HALE V. P., MCSWEEN H. Y., JR. AND MCKAY G. A. (1999) Re-evaluation of intercumulus liquid composition and oxidation state for the Shergotty meteorite. *Geochim. Cosmochim. Acta* **63**, 1459–1470.

HARVEY R. P., WADHWA M., MCSWEEN H. Y., JR. AND CROZAZ G. (1993) Petrography, mineral chemistry, and petrogenesis of Antarctic shergottites LEW 88516. *Geochim. Cosmochim. Acta* **57**, 4769–4783.

HERD C. D. K., PAPIKE J. J. AND BREARLEY A. J. (2001) Oxygen fugacity of martian basalts from electron microprobe, oxygen, and TEM-EELs analyses of iron-titanium oxides. *Am. Mineral.* **86**, 1015–1024.

JAGOUTZ E. (1989) Sr and Nd isotopic systematics in ALHA77005: Age of shock metamorphism in shergottites and magmatic differentiation on Mars. *Geochim. Cosmochim. Acta* **53**, 2429–2441.

JERRAM D. A., CHEADLE M. J., HUNTER R. H. AND ELLIOT M. T. (1996) The spatial distribution of grains and crystals in rocks. *Contrib. Mineral. Petrol.* **125**, 60–74.

LENTZ R. C. F. AND MCSWEEN H. Y., JR. (2000) Crystallization of the basaltic shergottites: Insights from crystal size distribution (CSD) analysis of pyroxenes. *Meteorit. Planet. Sci.* **35**, 919–928.

LONGHI J. AND PAN V. (1989) The parent magmas of the SNC meteorites. *Proc. Lunar Planet. Sci. Conf.* **19th**, 451–464.

MARSH B. D. (1988) Crystal size distribution (CSD) in rocks and the kinetics and dynamics of crystallization: I. Theory. *Contrib. Mineral. Petrol.* **99**, 277–291.

MCCOY T. J. AND LOFGREN G. E. (1999) Crystallization of the Zagami shergottite: An experimental study. *Earth Planet. Sci. Lett.* **173**, 397–411.

MCCOY T. J., TAYLOR G. J. AND KEIL K. (1992) Zagami: Product of two-stage magmatic history. *Geochim. Cosmochim. Acta* **56**, 3571–3582.

MCKAY G. A. (1986) Crystal/liquid partitioning of REE in basaltic systems: Extreme fractionation of REE in olivine. *Geochim. Cosmochim. Acta* **50**, 69–79.

MCSWEEN H. Y., JR. (1994) What we have learned about Mars from SNC meteorites. *Meteoritics* **29**, 757–779.

MCSWEEN H. Y., JR. (2002) The rocks of Mars, from far and near. *Meteorit. Planet. Sci.* **37**, 7–25.

MCSWEEN H. Y., JR. AND JAROSEWICH E. (1983) Petrogenesis of the Elephant Moraine A79001 meteorite: Multiple magma pulses on the shergottite parent body. *Geochim. Cosmochim. Acta* **47**, 1501–1513.

MEYER C. (1998) *Mars Meteorite Compendium—1998.* NASA, Lyndon B. Johnson Space Center, Houston, Texas, USA. 237 pp.

MIKOUCHI T. AND MIYAMOTO M. (2001) Dhofar 019 shergottite: Mineralogy and petrology of a new member of the basaltic martian meteorites (abstract). *Lunar Planet. Sci.* **32**, #1644, Lunar and Planetary Institute, Houston, Texas, USA (CD-ROM).

MITTLEFEHLDT D. W., LINDSTROM D. J., LINDSTOM M. M. AND MARTINEZ R. R. (1999) An impact-melt origin for lithology A of martian meteorite Elephant Moraine A79001. *Meteorit. Planet. Sci.* **34**, 357–367.

NEAL C. R., TAYLOR L. A., ELY J. C., JAIN J. C. AND NAZAROV M. A. (2001) Detailed geochemistry of new shergottite, Dhofar 019 (abstract). *Lunar Planet. Sci.* **32**, #1671, Lunar and Planetary Institute, Houston, Texas, USA (CD-ROM).

ONORATO P. I. K., UHLMANN D. R., TAYLOR L. A., COISH R. A. AND GAMBLE R. P. (1978) Olivine cooling speedometers. *Proc. Lunar Planet. Sci. Conf.* **9th**, 613–628.

PAPIKE J. J., TAYLOR L. A. AND SIMON S. (1991) Lunar materials. In *Lunar Sourcebook* (eds. G. Heiken, D. Vaniman and B. M. French), pp. 121–181. Cambridge University Press, New York, New York, USA.

RUBIN A. E., WARREN P. H., GREENWOOD J. P., VERISH R. S., LESHIN L. A. AND HERVIG R. L. (2000) Petrology of Los Angeles: A new basaltic shergottite find (abstract). *Lunar Planet. Sci.* **31**, #1963, Lunar and Planetary Institute, Houston, Texas, USA (CD-ROM).

SHEARER C. K., PAPIKE J. J., TAYLOR L. A. AND NAZAROV M. A. (2000) Trace element crystal chemistry of magmatic minerals in a new sample of the martian crust: Dhofar 019 (abstract). *Geol. Soc. Am.* **32**, A239.

SHEARER C. K., TAYLOR L. A. AND NAZAROV M. A. (2001) Trace element crystal chemistry of minerals in Dhofar 019. Implications for the petrogenesis of martian magmas (abstract). *Lunar Planet. Sci.* **31**, #1881, Lunar and Planetary Institute, Houston, Texas, USA (CD-ROM).

SMITH J. V. AND HERVING R. L. (1979) Shergotty meteorite: Mineralogy, petrography and minor elements. *Meteoritics* **14**, 121–142.

SMITH J. V., STEEL I. M. AND LEITCH C. A. (1983) Mineral chemistry of the shergottites, nakhlites, Chassigny, Brachina, pallasites and ureilites. *Proc. Lunar Planet. Sci. Conf.* **14th**, B229–B236.

STOLPER E. AND MCSWEEN H. Y., JR. (1979) Petrology and origin of the shergottite meteorites. *Geochim. Cosmochim. Acta* **43**, 1475–1498.

TAYLOR L. A. (1970) Low-temperature phase relations in the Fe-S system. *Carnegie Inst. Wash. YearBook* **68**, 259–270.

TAYLOR L. A. AND MISRA K. C. (1975) Pyroxene-phyric basalt 15075: Petrology and petrogenesis. *Proc. Lunar Sci. Conf.* **6th**, *Geochim. Cosmochim. Acta* **6 (Suppl.)** 165–179.

TAYLOR L. A., KULLERUD G. AND BRYAN W. B. (1971) Opaque mineralogy and shock features of Apollo 12 samples and a comparison with Apollo 11 rocks. *Proc. Lunar Sci. Conf.* **2nd**, *Geochim. Cosmochim. Acta* **2 (Suppl.)**, 855–871.

TAYLOR L. A., ONORATO P. I. K. AND UHLMANN D. R. (1977) Cooling rate estimations based on kinetic modeling of the Fe-Mg diffusion in olivine. *Proc. Lunar Sci. Conf.* **8th**, *Geochim. Cosmochim. Acta* **8 (Suppl.)**, 1581–1592.

TAYLOR L. A., ONORATO P. I. K., UHLMANN D. R. AND COISH R. A. (1978) Subophitic basalts from Mare Crisium: Cooling rates. In *Mare Crisium: The Views from Luna 24* (eds. R. B. Merrill and J. J. Papike), pp. 473–482. Pergamon Press, Elmsford, New York, USA.

TAYLOR L. A., PATCHEN A., TAYLOR D-H., CHAMBERS J. J. AND MCKAY D. S. (1996) X-ray digital imaging and petrography of lunar mare soils: Data input for remote sensing calibrations. *Icarus* **124**, 500–512.

TAYLOR L. A., NAZAROV M. A., IVANOVA M. A., PATCHEN A., CLAYTON R. N. AND MAYEDA T. N. (2000) Petrology of the Dhofar 019 shergottite (abstract). *Meteorit. Planet. Sci.* **35 (Suppl.)**, A155.

TREIMAN A. H., DRAKE M. J., JANSSENS M-J., WOLF R. AND EBIHARA M. (1986) Core formation in the Earth and the shergottite parent body (SPB): Chemical evidence from basalts. *Geochim. Cosmochim. Acta* **50**, 1001–1015.

TREIMAN A. H., MCKAY G. A., BOGARD D. D., MITTLEFEHLDT D. W., WANG M-S., KELLER L., LIPSCHUTZ M. E., LINDSTROM M. M. AND GARRISON D. (1994) Comparison of the LEW 88516 and ALHA77005 martian meteorites: Similar but distinct. *Meteoritics* **29**, 581–592.

WADHWA M. (2001) Redox state of Mars' upper mantle and crust from Eu anomalies in shergottite pyroxenes. *Science* **291**, 1527–1530.

WADHWA M., LENTZ R. C. F., MCSWEEN H. Y., JR. AND CROZAZ G. (2001) A petrologic and trace element study of Dar al Gani 476 and Dar al Gani 489: Twin meteorites with affinities to basaltic and lherzolitic shergottites. *Meteorit. Planet. Sci.* **36**, 195–208.

WARREN P. H., GREENWOOD J. P., RICHARDSON J. W., RUBIN A. E. AND VERISH R. S. (2000) Geochemistry of Los Angeles, a ferroan, La- and Th-rich basalt from Mars (abstract). *Lunar Planet. Sci.* **31**, #2001, Lunar and Planetary Institute, Houston, Texas, USA (CD-ROM).

ZIPFEL J., SCHERER P., SPETTEL B., DREIBUS G. AND SCHULTZ L. (2000) Petrology and chemistry of the new shergottite Dar al Gani 476. *Meteorit. Planet. Sci.* **35**, 95–106.